Sedimentologika

10.57035/journals/sdk.2026.e41.2335

Diagenetic evolution and reservoir quality of Aptian lacustrine resedimented deposits from the Santos Basin, Brazilian pre-salt

Mariane Cristina Trombetta* [1,2], **Sabrina Danni Altenhofen** [2], **Jaques Soares Schmidt** [2], **William da Silveira Freitas** [1,2], **Rosalia Barili** [2], **Amanda Goulart Rodrigues** [1], **and Luiz Fernando De Ros** [1]

[1]Institute of Geosciences of Federal University of Rio Grande do Sul, Porto Alegre, Rio Grande do Sul, Brazil
[2]Institute of Petroleum and Natural Resources of Pontifical Catholic University of Rio Grande do Sul, Porto Alegre, Rio Grande do Sul, Brazil

CRediT statement: *Writing-original draft*: MCT. *Writing-review & editing*: AGR, LFR. *Conceptualization*: RB. *Formal analysis*: MCT. *Methodology*: SDA, JSS, WSF. *Supervision*: AGR, LFR. *Funding acquisition*: RB.

*Corresponding author: Mariane Cristina Trombetta, marianetrombettta@gmail.com

Abstract

Pre-salt carbonate reservoirs of the Santos Basin, eastern Brazilian margin, contain giant hydrocarbon accumulations, with resedimented deposits constituting the highest-quality reservoirs across several oilfields. Despite their importance, the diagenetic evolution of the lacustrine resedimented deposits remains poorly understood. This study investigates the diagenetic patterns and controls on reservoir quality of the resedimented deposits of the Aptian Barra Velha Formation through integrated petrography, fluid inclusions, petrophysical, and micro-computed tomography (μCT) analysis. Reservoir petrofacies were characterized according to the main controls on porosity evolution, which comprised: dolomitization, silicification, and compaction. Dolomite and silica precipitation are multiphase, as evidenced by paragenetic relations, and by fluid inclusions data showing heterogeneous entrapment with wide homogenization temperature ranges. Blocky dolomite precipitated both before and after compaction, while late saddle dolomite formed during deeper burial. At least two eodiagenetic silicification phases occurred, followed by late diagenetic coarse quartz precipitation. The relative timing between compaction and eodiagenetic dolomite, silica and calcite precipitation fundamentally controls reservoir quality in the resedimented deposits. Mesodiagenetic and hydrothermal processes had subordinate influence on porosity evolution. Resedimented deposits show greater susceptibility to compaction than in situ deposits, owing to the more stable crystalline framework of the latter. This study provided essential insights to improve the reservoir characterization and optimize the development strategies for the pre-salt accumulations, as well as for understanding the diagenetic evolution of resedimented lacustrine carbonates worldwide.

Research Article

Executive Editor
Giovanna Della Porta

Associate Editor
Arnaud Gallois

Reviewers
Youri Hamon
one anonymous reviewer

Production Manager
Jarred Lloyd

Production Assistant
Miguel Ángel

Copy Editor
Sara Biddle

Received: 2025-09-06
Accepted: 2025-12-26
Published: 2026-04-16

Keywords
lacustrine diagenesis
pre-salt reservoirs
re-sedimented deposits
petrofacies

Plain language summary

Brazil pre-salt carbonate rocks host one of the largest oil and gas reserves in the world. Resedimented deposits, which constitute excellent reservoirs in the succession, show a complex evolution that control their quality. This study combines systematic petrography, fluid inclusion analysis, and microtomography to understand the impact of dissolution, compaction, dolomite and silica precipitation on the porosity of the intraclastic rocks. We found that the timing of these processes strongly controls the pore space available for oil and gas. These findings contribute to reduce the exploration uncertainties of pre-salt reservoirs and may help to understand similar lacustrine carbonate rocks globally.

Resumo

Os reservatórios carbonáticos do pré-sal da Bacia de Santos, na margem leste brasileira, contêm acumulações gigantes de hidrocarbonetos, sendo que os depósitos ressedimentados constituem os reservatórios de mais alta qualidade em diversos campos de petróleo. Apesar de sua importância, a evolução diagenética dos depósitos lacustres ressedimentados ainda é pouco compreendida. Este estudo investiga os padrões diagenéticos e os controles sobre a qualidade de reservatório dos depósitos ressedimentados da Formação Barra Velha (Aptiano), por meio da integração de análises de petrografia, inclusões fluidas, propriedades petrofísicas e microtomografia computadorizada (μCT). As petrofácies de reservatório foram caracterizadas de acordo com os principais controles sobre a evolução da porosidade, que incluem: dolomitização, silicificação e compactação. A precipitação de dolomita e sílica ocorre em múltiplas fases, conforme evidenciado pelas relações paragenéticas e pelos dados de inclusões fluidas, que indicam aprisionamento heterogêneo com ampla variação nas temperaturas de homogeneização. A dolomita blocosa precipitou tanto antes quanto após a compactação, enquanto a dolomita em sela se formou durante soterramento mais profundo. Pelo menos duas fases de silicificação eodiagenética foram identificadas, seguidas pela precipitação tardia de quartzo macrocristalino. O tempo relativo entre a compactação e a precipitação eodiagenética de dolomita, sílica e calcita controla fundamentalmente a qualidade dos reservatórios nos depósitos ressedimentados. Processos mesodiagenéticos e hidrotermais tiveram influência subordinada na evolução da porosidade. Os depósitos ressedimentados apresentam maior suscetibilidade à compactação em comparação aos depósitos in situ, devido ao arcabouço cristalino mais estável destes últimos. Este estudo fornece insights essenciais para aprimorar a caracterização de reservatórios e otimizar estratégias de desenvolvimento das acumulações do pré-sal, além de contribuir para a compreensão da evolução diagenética de carbonatos lacustres ressedimentados em escala global.

Resumo em linguagem simples

As rochas carbonáticas do pré-sal brasileiro abrigam uma das maiores reservas de petróleo e gás do mundo. Os depósitos ressedimentados, que constituem excelentes reservatórios na sucessão, apresentam uma evolução complexa que controla sua qualidade. Este estudo combina petrografia sistemática, análise de inclusões fluidas e microtomografia para compreender o impacto da dissolução, compactação e da precipitação de dolomita e sílica na porosidade das rochas intraclásticas. Verificou-se que o momento relativo (timing) desses processos controla fortemente o espaço poroso disponível para acumular petróleo e gás. Esses resultados contribuem para reduzir as incertezas exploratórias em reservatórios do pré-sal e podem auxiliar na compreensão de rochas carbonáticas lacustres análogas em escala global.

1 Introduction

Lacustrine carbonate deposits represent dynamic systems that are particularly sensitive to subtle environmental changes (Platt & Wright, 1991; Tucker & Wright, 2009; Wright, 2012). These deposits commonly exhibit more complex vertical stacking patterns and horizontal distribution than those of marine carbonates. The inherent complexity of lacustrine systems poses significant challenges for their hydrocarbon exploration, demanding the integration of multiple scales and analytical techniques. During the last decades, the exploration of the giant South Atlantic pre-salt carbonate reservoirs has been driving the

increasing prominence of these unique lacustrine deposits.

The lacustrine reservoirs of the pre-salt sag succession are essentially composed of carbonates, magnesian clays and silica, including both in situ precipitates and resedimented deposits. Although some authors have interpreted the pre-salt in situ lithologies as microbial deposits (e.g., Araújo et al., 2022; Gomes et al., 2024; Sabato Ceraldi & Green, 2016; Saller et al., 2016), the genesis of the in situ precipitates has been mostly interpreted as abiotic, based on petrographic and isotopic evidence (Carvalho et al., 2022; De Ros, 2018, 2021; Farias et al., 2019; Gomes et al., 2020; Lima & De Ros, 2019; Pietzsch et al., 2018, 2020; Schrank et al., 2024; Wright, 2022; Wright & Barnett, 2015, 2017; Wright & Tosca, 2016). The resedimented deposits contain carbonate fragments derived from in situ deposits (intraclasts) produced by the action of gravitational processes (Barnett et al., 2021), waves (De Medeiros et al., 2024), or internal waves in a stratified lacustrine system (Altenhofen et al., 2024, 2026).

Both the in situ and resedimented deposits are relevant reservoirs in the pre-salt section, reaching 2 981 million bbl/d of oil and 139.79 million m^3/d of natural gas (Agência Nacional do Petróleo, 2025a). The porosity of the resedimented carbonates is predominantly primary, whereas in many in situ rocks it was largely generated by matrix dissolution (Herlinger et al., 2017; Schrank et al., 2024; Wright & Barnett, 2015). Nevertheless, diagenetic alterations such as cementation, dolomitization, silicification, and compaction significantly impacted the reservoir quality of the resedimented deposits (Carvalho et al., 2022), justifying studies for the development of geologically coherent models for these reservoirs. Although the diagenesis of the pre-salt rocks has been the subject of numerous recent publications, studies specifically focused on the resedimented carbonates remain very scarce. The primary textural and compositional variations within the resedimented deposits and their diagenetic evolution form reservoirs with very distinct characteristics (Herlinger et al., 2017). In addition to numerous eodiagenetic modifications, mesodiagenetic processes were responsible for porosity reduction in some cases, while in others promoting the development of zones with intense fracturing and dissolution, which resulted in exceptionally well-connected reservoirs (Fernández-Ibáñez, Jones, et al., 2022; Fernández-Ibáñez, Nolting, et al., 2022). In our study, eodiagenetic and mesodiagenetic were used according to the original definition sensu Choquette & Pray (1970), which is of surface-influenced fluids and temperatures for eodiagenetic processes, and burial-controlled modifications, for mesodiagenetic processes.

The high degree of heterogeneity and the wide distribution of these reservoirs throughout the Aptian pre-salt succession highlight the importance of systematically examining their diagenesis through integrated studies. This article presents a study of the diagenesis of Santos Basin resedimented pre-salt deposits, developed with an integrated approach, combining sedimentary characterization, petrography, fluid inclusions and petrophysical analysis, including micro-computed tomography (μCT), to better understand the evolution of the pore systems of these reservoirs. Our study provides new insights on the multiple factors favoring the reduction, preservation or enhancement of reservoir quality in the resedimented pre-salt, as well as in equivalent resedimented lacustrine carbonates.

2 Geological setting

The Santos Basin, offshore SE margin of Brazil, covers an area of approximately 350 000 km^2 down to a bathymetric depth of 3 000 m (Moreira et al., 2007). The studied wells are located in three fields in the northeastern and central part of the Santos Basin (Figure 1). The Cabo Frio High separates the Santos Basin from the Campos Basin to the north, while the Florianópolis High marks its southern boundary with the Pelotas Basin (Moreira et al., 2007).

Like other basins along the Brazilian eastern margin, the Santos Basin originated during the opening of the South Atlantic Ocean (Mohriak et al., 2008). The sedimentary infill comprises three supersequences: rift, post-rift (sag), and drift (Figure 2). The pre-salt play encompasses the supersequences formed during the rift and post-rift stages. The rift supersequence (Hauterivian to lower Aptian) is subdivided into lower and upper intervals (Moreira et al., 2007). In the lower interval, extensive basaltic volcanism constituted the Camboriú Formation (Dias, 2005; Quirk et al., 2013). During the upper rift interval, deep half-grabens were infilled with alluvial siliciclastic sediments and lacustrine deposits of kerolite-stevensite ooids from the Piçarras Formation (De Oliveira Nardi Leite et al., 2020; Moreira et al., 2007; Pietzsch et al., 2018), covered by bivalve bioclastic limestones (”coquinas”)

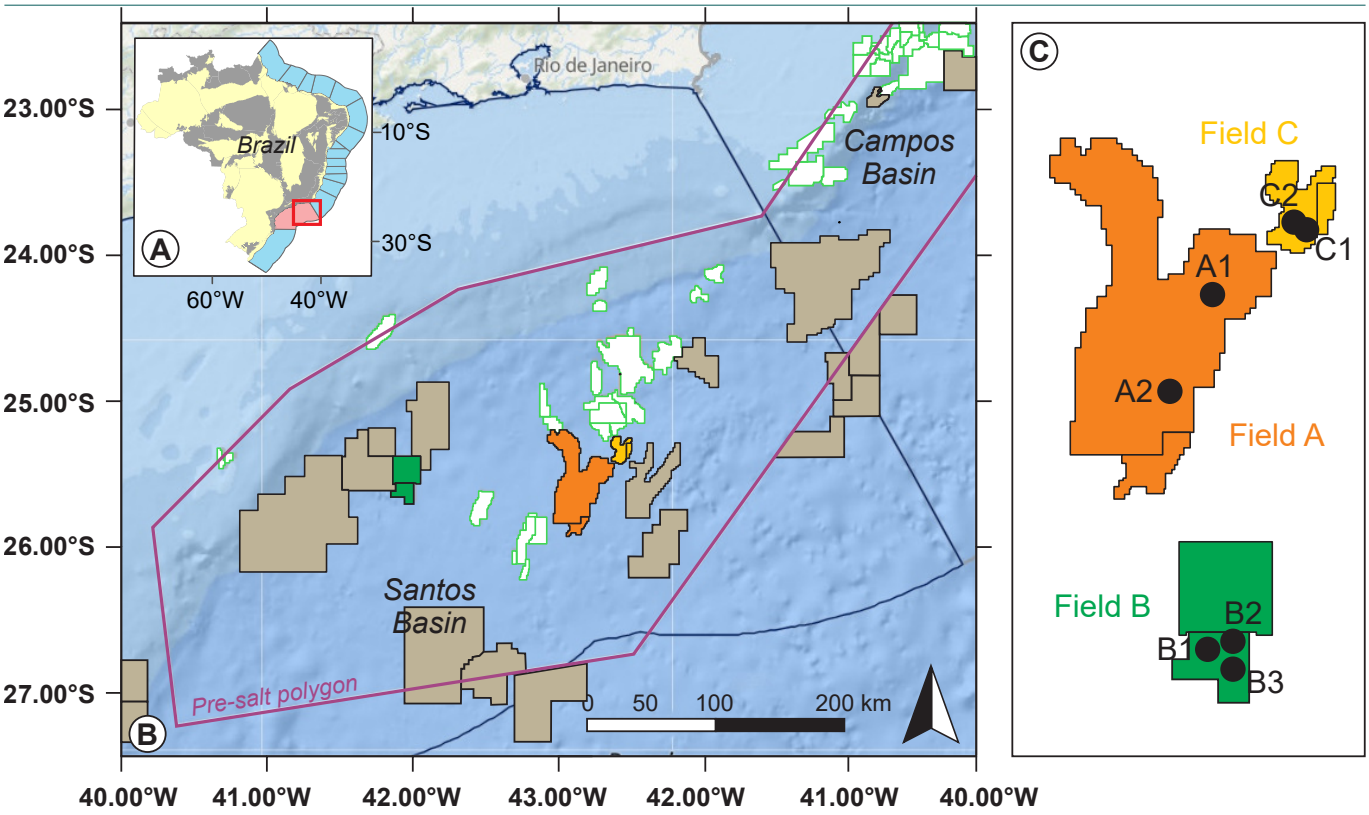

Figure 1 – Location of study area. **(A)** Santos Basin. **(B)** Exploration and production blocks from Santos Basis (modified from Agência Nacional do Petróleo, 2025b). **(C)** Location of the seven wells in the three studied fields.

and organic-rich shales of the Itapema Formation (Szatmari & Milani, 2016). The Aptian post-rift phase is represented by the Barra Velha Formation, limited at the base by the Pre-Alagoas Unconformity and at the top by the salt base unconformity (Moreira et al., 2007).

The unusual in situ deposits of the Barra Velha Formation are constituted by spherulitic and fascicular calcite aggregates precipitated in a magnesian clay matrix. They were initially interpreted as microbial stromatolites (Moreira et al., 2007; Terra et al., 2010) and later reinterpreted as a product of chemical abiotic precipitation (e.g., Carramal et al., 2022; Farias et al., 2019; Gomes et al., 2020; Pietzsch et al., 2020; Schrank et al., 2024; Wright, 2022; Wright & Barnett, 2015; Wright & Rodriguez, 2018). Resedimented deposits that occur associated with the in situ deposits are represented by intraclastic calcirudites and calcarenites formed by the erosion, reworking and redeposition of the in situ deposits (Altenhofen et al., 2024, 2026; Barnett et al., 2021; De Medeiros et al., 2024). During the late Aptian, the rupture of the Florianópolis High barrier allowed the inflow of marine waters, and the deposition of the thick evaporitic sequence of the Ariri Formation. After the deposition of shallow to deep marine carbonate sediments during the Albian, the upper portion of the drift sequence comprises marine shales with turbiditic sands in deeper areas, as well as proximal sandy and gravel marginal deposits (Moreira et al., 2007).

The Santos Basin hosts major petroleum systems, including the pre-salt play that currently accounts for 78.8 % of petroleum production in the country (Agência Nacional do Petróleo, 2025a). The pre-salt play encompasses the rift and post-rift megasequences, including the Itapema and Barra Velha Formations. The thick evaporitic sequence of the Ariri Formation serves as an effective seal for these reservoirs with giant hydrocarbon accumulations.

3 Methods and materials

Intervals with occurrence of resedimented deposits were studied in seven wells from three pre-salt oilfields of the Santos Basin (Figure 1). The name of the fields and exact position of the wells cannot be disclosed due to data confidentiality. Fields were named as A, B and C, and wells as A-1, A-2 (from field A), B-1, B-2, B-3 (from field B), C-1, C-2 (from field C). A total of 1121 thin sections were analyzed from the seven wells. Of these, 328 samples corresponding to resedimented carbonates were systematically characterized. They were prepared from 132 core trim, 83 core plugs, and

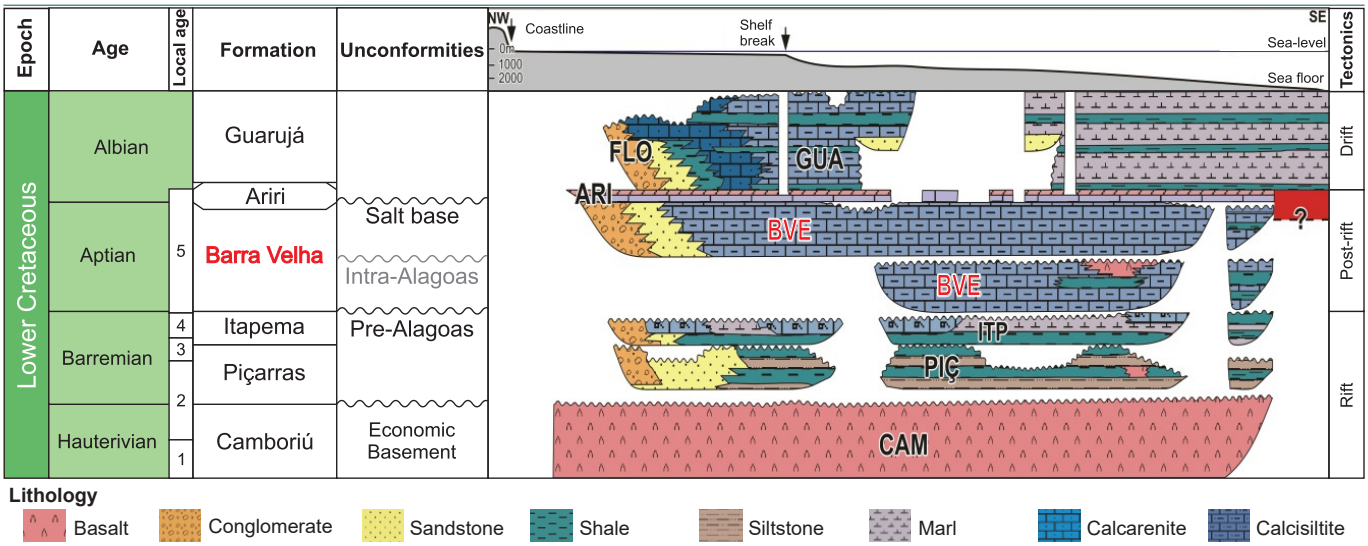

Figure 2 – Lower Cretaceous stratigraphic chart of the Santos Basin. The Barra Velha Formation is highlighted in red (BVE). Lithostratigraphic units: Camboriú Formation (CAM); Piçarras Formation (PIÇ); Ariri Formation (ARI); Guarujá Formation (GUA); Florianópolis Formation (FLO). Local ages: Rio da Serra (1); Aratu (2); Buracica (3); Jiquiá (4); Alagoas (5). Modified from Moreira et al. (2007).

113 sidewall samples impregnated with blue epoxy resin. Staining with Alizarin red-S and potassium ferricyanide solution was applied to all thin sections to differentiate the carbonate minerals, as outlined by Dickson (1965).

Systematic petrographic analysis was performed in the Rock Characterization Laboratory of the Institute of Petroleum and Natural Resources (IPR-PUCRS) using the Petroledge® software (De Ros et al., 2007). The petrographic analysis records the volume, location and the paragenetic relations of each observed primary and diagenetic constituent, and pore type. The classification of the resedimented deposits followed the system proposed by De Ros & Oliveira (2023). Pore types were classified according to Choquette & Pray (1970). Zeiss Axio Imager A1 and Leica DM750P microscopes were used to perform petrographic analyses. Ultraviolet epifluorescence analysis was conducted on 10 thin sections using a Zeiss HXP 120 V metal halide fluorescence light source, connected to an Axio Imager A2 microscope with set 02 (excitation G 365 nm, beamsplitter FT 395 nm, emission LP 420 nm) and blue-cyan Lumar 09 filters (excitation BP 450 to 490 nm, emission LP 515 nm). In addition, twenty-three thin sections were selected for automated mineralogical distribution mapping using a QEMSCAN 650 (FEI) equipment with two coupled EDS/Bruker detectors at the University of Brasilia.

Fluid inclusions (FI) petrography and microthermometry were performed on four double-polished thin sections (120 µm-thick). FIs were analyzed in prismatic quartz, blocky, matrix-replacive, saddle dolomite, and macrocrystalline calcite. A total of 109 determinations of homogenization temperature (*Th*) were conducted by H-Expertise Services S.A.S (H-ES, Vandœuvre-lès-Nancy, France) and by Fluid Inclusion Technologies Schlumberger (FIT-SLB, Texas, USA). At GeoRessources laboratory (University of Lorraine, France), measurements were conducted using a LINKAM MDS 600 heating-freezing stage, operating between −170 to 400 °C, coupled with a Sony Exwave HAD3 color video camera mounted on an Olympus BX51 microscope. At FIT-SLB, analyses were performed using a Fluid Inc. USGS-type heating-freezing stage. Both microthermometric systems were thermally calibrated using synthetic fluid inclusion standards. The analytical precision is estimated to be ± 0.2 °C for ice melting temperatures (Tm_{ice}) and ± 0.5 °C for homogenization temperatures (*Th*). Fluid inclusion assemblages (FIAs) were classified following the methodology of Roedder (1984), according to their genetic types (primary, secondary, or pseudo-secondary) and correlated with the paragenetic sequence.

The homogenization temperature (*Th*) indicates when a biphasic FI with a liquid phase volume greater than the vapor phase at room temperature homogenizes to a single liquid phase after heating. The vapor homogenization temperature (Th_{vapor}) highlights cases when a biphasic FI with a vapor phase volume greater than the liquid phase at room temperature homogenizes as a single vapor phase after heating.

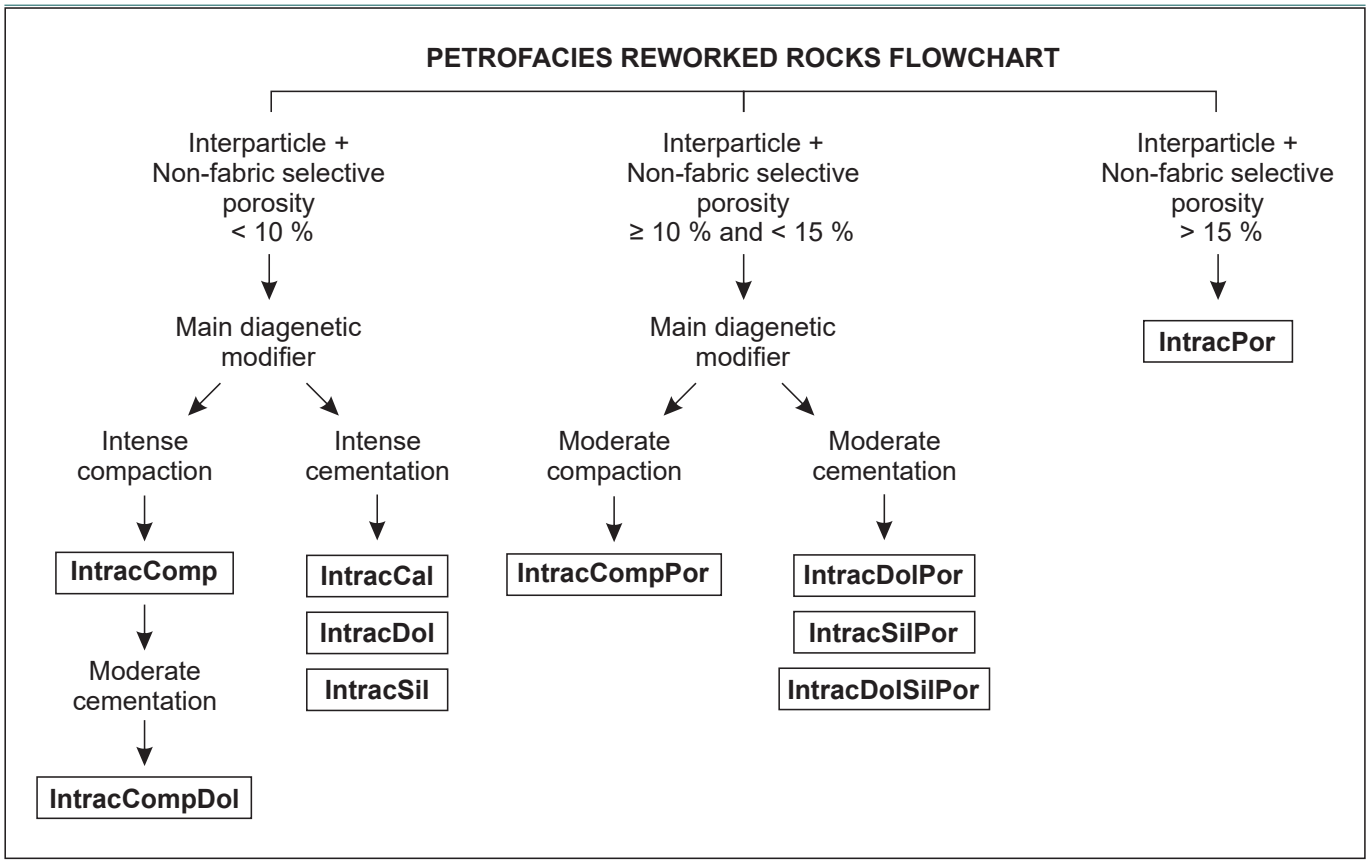

Figure 3 – Schematic representation of the workflow used for the definition of reservoir petrofacies in the studied resedimented pre-salt deposits. First, the resedimented "intraclastic" deposits were grouped according to interparticle porosity values combined with the contribution of non-fabric selective porosity (e.g., vugs and channels). Subsequently, suffixes were assigned based on the main diagenetic process affecting porosity.

Reservoir petrofacies sensu De Ros & Goldberg (2007) were defined by the combination of the main textural and fabric features, primary composition, and diagenetic processes and products that mostly control the pore system. Attributes that significantly impacted the porosity and permeability were used as grouping criteria. Resedimented petrofacies are identified by the prefix 'Intrac' (from intraclastic), due to the dominantly intraclastic origin of the carbonate particles. After an initial grouping of the samples, the preliminary petrofacies were evaluated against petrophysical parameters using statistical tools. The porosity reduction by compaction and cementation was evaluated on an Ehrenberg (1995) diagram. Samples with compaction as the main porosity reduction process were given the suffix 'Comp'. Samples whose porosity was mostly controlled by cementation were assigned with the suffixes 'Dol', 'Cal', and 'Sil', depending on whether dolomite, calcite, or silica, respectively, were the main diagenetic modifiers. Petrofacies with two significant diagenetic porosity modifiers (considered when the difference between their volumes is less than 5 %) were labeled with both mnemonic suffixes (e.g., DolSil for dolomite and silica; Figure 3).

Routine core analysis (RCA) data, including porosity and permeability measurements, were obtained from the National Agency of Petroleum, Natural Gas and Biofuels (ANP) database. Computerized X-ray microtomography was performed in the Rock Characterization Laboratory of the Institute of Petroleum and Natural Resources (IPR-PUCRS), using a SkyScan 1173 system equipped with a micro-focus X-ray source operating at 130 kV and 61 µA. To minimize beam hardening effects, a 0.25 mm brass filter was applied. Image acquisition was carried out with pixel resolutions ranging from 7 to 35.7 µm. Each sample was scanned over a rotational range of 270° to 360°, with an angular step of 0.2°, generating 16-bit TIFF transmission images at each increment. Three-dimensional reconstruction was conducted using a cone-beam algorithm, optimized for variations in sample thickness. Image processing and quantitative analysis, including segmentation, pore and pore throat identification, dimensional measurements, and total

and partial volume calculations, were carried out using AVIZO Thermo Scientific software.

4 Results

4.1 Distribution of resedimented deposits

The analysis of the total 1121 thin sections allowed us to understand the stratigraphic distribution of the resedimented deposits across the three studied fields (Figure 4). The thin sections were grouped into six major rock types (Table 1), and the proportion of each one is indicated in parentheses: in situ deposits (572 samples; 51.1 %), resedimented deposits (331 samples; 29.6 %), crystalline rocks (115 samples; 10.3 %), mudstones (66 samples; 5.9 %), microbial deposits (29 samples; 2.6 %), and anhydrite (6 samples; 0.5 %). As can be observed in Figure 4, the resedimented deposits are intercalated in high frequency with the in situ deposits, and with crystalline or microbial deposits. The resedimented deposits occur as layers that range from millimeter-scale laminations, locally interbedded with in situ deposits, to thick depositional units reaching approximately 10 m in thickness in some locations. Also, it is visible that there is a greater representation of resedimented deposits in Field C compared to the other fields.

The resedimented carbonates were texturally classified (Figure 5) into calcarenites (108 samples; 32.6 %), rudaceous calcarenites (64 samples; 25.4 %), slightly rudaceous calcarenites (63 samples; 19 %), arenaceous calcirudites (47 samples; 14.2 %), calcirudites (8 samples; 2.4 %), muddy calcirudites (5 samples; 1.51 %), and muddy calcarenites (3 samples; 0.9 %). In addition to these carbonate rocks, hybrid carbonate-siliciclastic arenites (10 samples; 3 %) and breccias (3 samples; 0.9 %) were also characterized.

4.2 Primary composition and texture of the resedimented deposits

The resedimented deposits from the studied wells are primarily composed of intraclasts eroded from the characteristic in situ pre-salt deposits. These comprise mostly intraclasts of spherulitic and fascicular calcite aggregates, as well as intraclasts of macro- and microcrystalline calcite. Microbial intraclasts with a clotted texture, along with dolomitic, siliceous, and muddy intraclasts, occur locally. The intraclasts range from 0.1 to 3.5 m in diameter, predominantly with medium to coarse sand size, and from well-rounded to angular, predominantly sub-rounded shape. They commonly exhibit moderate sorting. The average intraclast content among the studied samples is 46.4 %, with a maximum of 79 %, indicating their predominance in the composition (Table 2; Figure 6A-E).

Other primary constituents include clay ooids with carbonate intraclastic or volcanic nuclei covered by irregular Mg-clay envelopes (Figure 6F; Altenhofen et al., 2024; Carramal et al., 2022). The ooids often exhibit single superficial clay envelopes that have been replaced and expanded by calcite or dolomite. In some cases, these envelopes were detached from their nuclei. The bioclasts identified are articulated and disarticulated ostracods and undetermined phosphatic bioclasts. Carbonate and phosphate bioclasts sometimes occur concentrated in levels, and are often found within spherulitic and fascicular intraclasts, having been engulfed during the in situ growth of the calcite aggregates.

A magnesian clay matrix locally fills the interparticle porosity in the resedimented deposits, but it also occurs segregated in laminations intercalated with the intraclastic levels (Figure 6B). This matrix consists of a clay-size fraction as well as silt and fine sand-size clay peloids. It is often replaced by blocky dolomite or cryptocrystalline silica. Locally, the matrix contains significant amounts of detrital silt, such as quartz, feldspar, micas, and celadonite grains. Clay intraclasts are rarely found. They occur mixed with carbonate particles and are commonly replaced by dolomite. Compacted clay intraclasts locally fill interparticle porosity as clay pseudomatrix.

4.3 Diagenetic phases

Dolomite, silica, and calcite are the main diagenetic constituents in the resedimented carbonate reservoirs. Dolomite is the main diagenetic constituent in six of the seven wells. Only Well C1 contains a silica content higher than dolomite. The volume of diagenetic calcite is limited, standing out only in Well A2 as macrocrystalline (> 0.12 m) interparticle cement. Macrocrystalline calcites commonly fill fractures in calcite intraclasts. Locally, calcite occurs as a microcrystalline replacement constituent, replacing and displacing the clay envelopes of ooids. Some samples display rims of blocky calcite covering the intraclasts.

Blocky dolomite occurs abundantly, both as an intraparticle constituent, replacing calcite intraclasts

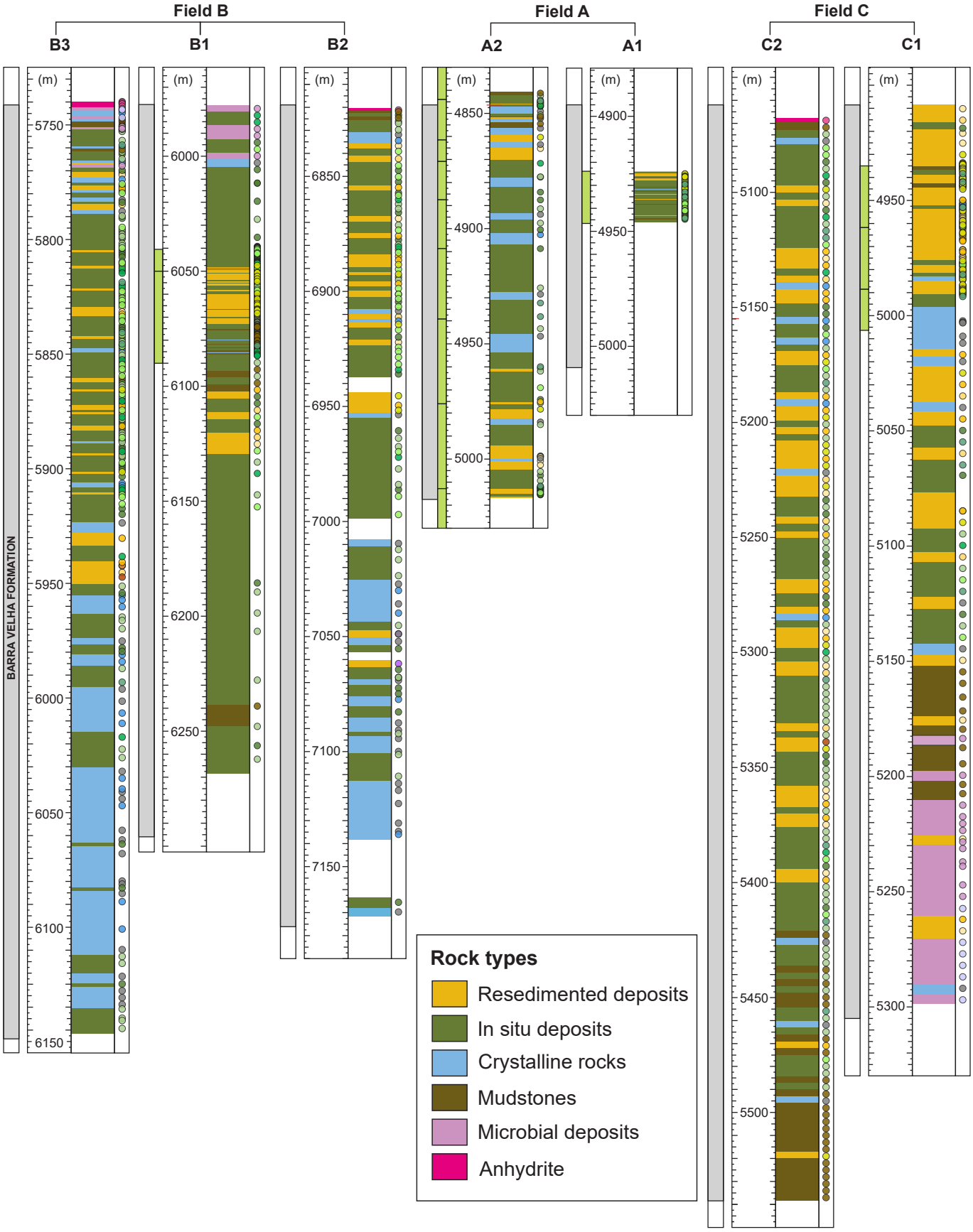

Figure 4 – Schematic representation of the distribution of rock types in the seven studied wells. Vertical scale in meters. Gray bars indicate Barra Velha Formation thickness based on ANP well data. Green bars correspond to cored intervals.

Table 1 – Rock type classification with sample distribution and main characteristics.

Rock type	Number of Samples	Proportion (%)	Main characteristics
In situ deposits	572	51.12	In situ deposits are formed by diagenetic and/or syngenetic shrubs and spherulitic calcite associated with magnesian clay. These deposits exhibit layers with thicknesses ranging from centimeters to meters. In situ deposits commonly display irregular to plane-parallel laminations and variable degrees of coalescence of the calcite precipitates.
Resedimented deposits	331	29.58	Resedimented deposits consist mainly of intraclastic carbonate particles derived from the erosion and redeposition of previously deposited carbonates. They are predominantly massive or locally plane-parallel laminated, medium- to coarse-grained, composed of subrounded to rounded particles, and show moderate sorting.
Crystalline rocks	115	10.28	Intensely silicified or dolomitized rocks in which original textures are no longer preserved. They are represented by dolostones and cherts, with thicknesses ranging from centimeters to meters, and are concentrated at the base of wells B2 and B3.
Mudstones	66	5.90	Mudstone composed of magnesian clay, commonly replaced by microcrystalline calcite. It occurs in millimeter- to centimeter-scale layers and exhibits irregular to plane-parallel lamination.
Microbial deposits	29	2.59	Carbonate deposits characterized by a grumose texture typical of microbial carbonates. They display stromatolitic to thrombolitic structures, with layer thicknesses ranging from centimeters to meters, and occur in isolated intervals at the base of well C1 and at the top of wells B1 and B3.
Anhydrite	6	0.54	Massive layers of evaporitic calcium sulfate, with thicknesses ranging from millimeters to centimeters, occurring at the upper boundary of the Barra Velha Formation in wells B2, B3, and C2.
Total	1119	100.00	

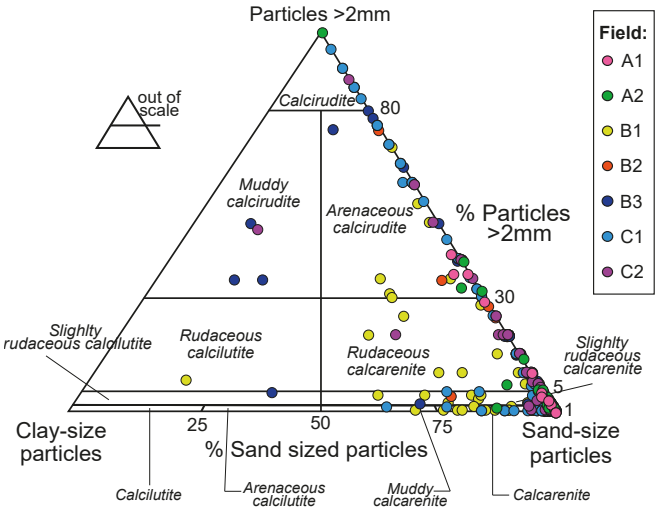

Figure 5 – Textural classification of resedimented deposits described from the seven studied wells (modified from De Ros & Oliveira, 2023).

and other primary constituents (34.5 %), and filling interparticle porosity (32.2 %; Figure 7A). In wells B1 and B3, blocky dolomite is also commonly observed replacing the clay matrix and pseudomatrix from the compaction of clay intraclasts (Figure 7B). Matrix-replacive blocky dolomite can be distinguished from blocky dolomite that fills primary interparticle porosity by the arrangement of the crystals. The replacive variety preserves some alignment reflecting the original lamination of the matrix, whereas the pore-filling dolomite typically nucleated along the edges of the particles, as also described by Schrank et al. (2024).

Blocky dolomite also largely replaced the clay peloids among the calcite intraclasts, as well as those included in the calcite aggregates. Saddle dolomite commonly occurs as a pore filling, but also as a matrix replacement constituent. Larger volumes of saddle dolomite occur in field B and in Well A2 (Figure 7C). Pseudomorphic dolomite replacement of the original calcite fabric of the intraclasts stands out in Well A2 (Figure 7D).

Silica habits include cryptocrystalline silica, microcrystalline quartz, fibrous-radiated chalcedony, as well as coarsely crystalline quartz (macrocrystalline, coarse mosaic, prismatic and drusiform; Figure 7E and F). Cryptocrystalline silica preferentially replaced the laminated clay matrix and peloids. Microcrystalline (< 0.12 m) quartz replaced the carbonate particles and filled the interparticle porosity, often obliterating the

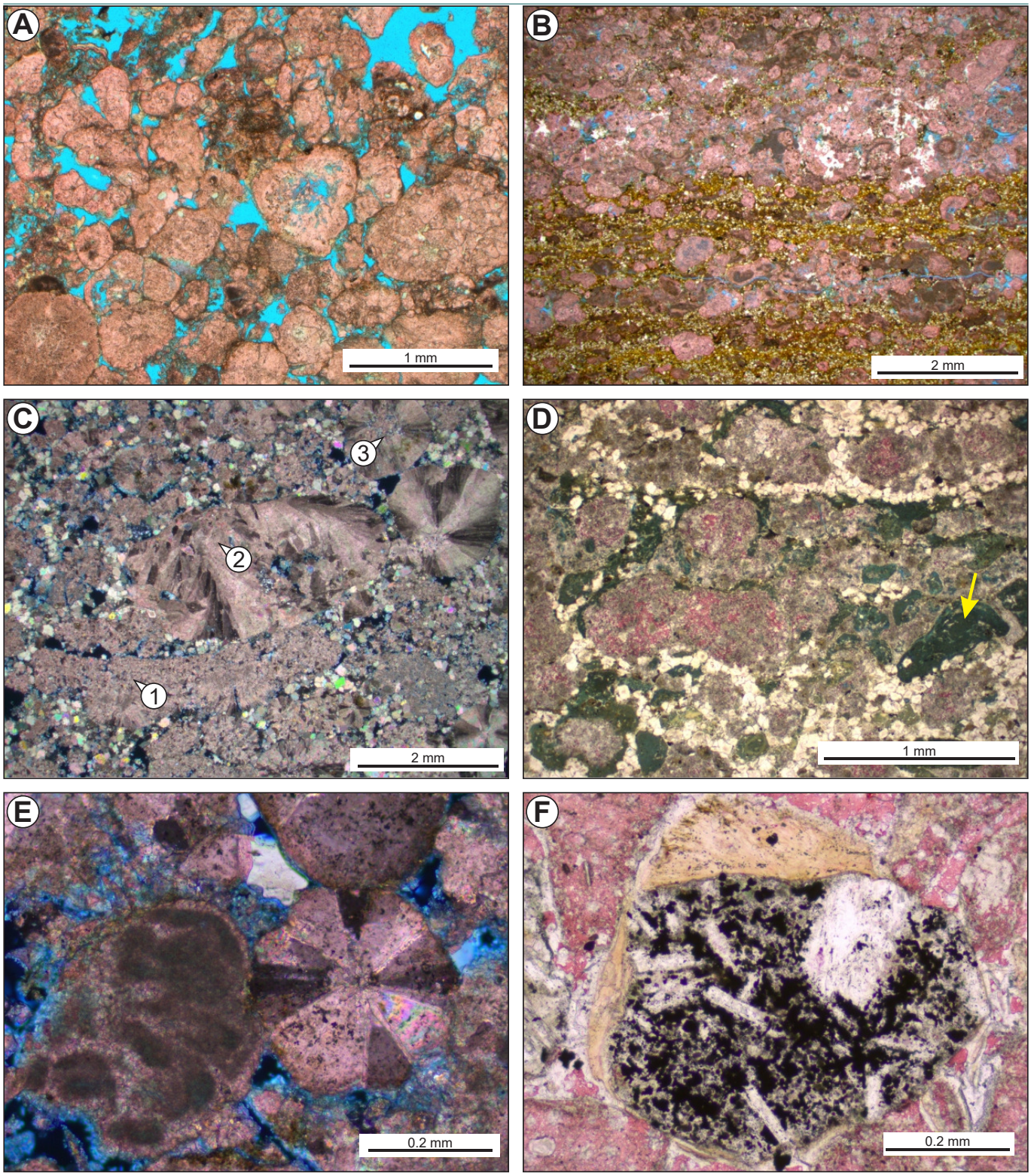

Figure 6 – Textural and compositional aspects of the analysed resedimented deposits. **(A)** Calcarenite composed of calcite intraclasts with preserved interparticle porosity. Uncrossed polarizers (//P). **(B)** Laminated intraclastic calcarenite with peloidal clay laminations intensely replaced by dolomite. Silica patches fill interparticle pores in the intraclastic laminae (//P). **(C)** Calcite intraclasts with macrocrystalline (1), fascicular (2), and spherulitic (3) textures. Blocky dolomite partially fills the interparticle porosity. Crossed polarizers (XP). **(D)** Hybrid calcarenite with partially dissolved clay intraclasts (yellow arrow) cemented by blocky dolomite (//P). **(E)** Intraclast with clotted texture, suggestive of microbial origin (left) and spherulitic intraclast (right; XP). **(F)** Clay ooid with volcanic nucleus, and a single discontinuous envelope (//P).

pre-compaction interparticle pore space. Chalcedony is abundant as cement in the resedimented deposits, commonly forming fibro-radiated aggregates and rims covering the carbonate particles, but also frequently replacing the framework constituents. Coarsely crystalline quartz mostly filled the dissolution

Table 2 – Summary of primary composition of described resedimented deposits.

Primary Constituent / Well	A1		A2		B1		B2		B3		C1		C2	
	Avg.	*Max.*	*Avg.*	*Max.*	*Avg.*	*Max.*	*Avg.*	*Max.*	*Avg.*	*Max.*	*Avg.*	*Max.*	*Avg.*	*Max.*
Clay Ooid	2.06	14.5	12.47	54.67	0.19	8.00	1.5	12.5	1.59	23.00	1.34	42.00	4.35	35.00
Spherulitic intraclast	12.05	25.00	7.02	20.67	25.65	50.00	15.78	37.00	13.94	45.00	16.41	63.00	20.1	50.00
Fascicular intraclast	17.72	38.00	3.73	15.5	15.55	48.00	10.98	32.00	15.51	45.00	16.9	52.00	13.89	33.5
Undiff intraclast	0.38	5.00	0.36	8.00	0.00	0.00	1.35	25.00	0.05	1.00	0.07	9.00	3.24	25.00
Microbial intraclast	0.00	0.00	0.47	8.00	0.00	0.00	0.00	0.00	1.34	12.00	1.3	68.5	0.06	2.5
Carbonate sand intraclast	0.92	7.00	0.00	0.00	0.00	0.00	0.00	0.00	0.00	0.00	0.00	0.00	0.00	0.00
Macrocrystalline intraclast	6.23	63.00	2.88	12.67	4.68	40.00	0.53	5.00	3.06	44.00	3.25	35.67	3.54	28.00
Microcrystalline intraclast	6.67	15.00	15.84	41.33	8.24	36.00	7.26	20.00	10.7	68.00	8.05	70.00	7.67	30.00
Dolomite intraclast	0.00	0.00	0.00	0.00	0.00	0.00	0.00	0.00	0.21	6.00	0.12	4.00	0.02	1.00
Total Carbonate intraclast	44.00	75.00	30.3	62.00	54.13	76.5	35.91	65.5	44.6	72.00	45.98	79.00	48.5	70.01
Detrital grains	0.05	0.67	0.98	13.00	1.44	5.25	0.53	3.5	0.32	2.5	0.05	2.5	0.14	1.5
Carbonate bioclast	0.05	0.67	0.09	2.00	0.02	1.00	0.09	1.00	0.01	0.33	0.2	3.00	0.21	5.00
Preserved Matrix	0.04	0.5	1.13	10.5	2.05	9.00	0.13	2.00	1.18	12.5	1.21	16.00	0.63	5.00
Mud intraclast	0.00	0.00	0.22	2.00	0.03	1.33	0.03	0.5	0.00	0.00	0.3	7.00	0.13	3.00
Phosphate bioclast	0.46	1.5	0.28	3.5	0.6	3.5	0.63	4.5	0.29	3.00	0.08	4.00	0.05	2.00
Siliceous intraclast	0.00	0.00	0.00	0.00	0.00	0.00	0.21	2.01	0.59	17.00	0.19	10.00	0.59	10.00

secondary porosity, such as vuggy, channel, and fracture pores. However, drusy and macrocrystalline quartz are also observed filling primary interparticle porosity.

Other diagenetic constituents are rare (max. 5 % of volume, in few samples) and consist of pyrite, dawsonite, barite and chlorite. Pyrite, the most abundant among these minor constituents, commonly occurs replacing clay matrix, peloids, and intraclasts with microcrystalline and framboidal habits. Dawsonite occurs in fibrous, fibro-radiated and, less commonly, prismatic forms, replacing matrix and locally filling dissolution porosity. Dawsonite is relatively common in field C but absent in field B. Prismatic barite occurs filling primary and secondary porosity. The occurrence of chlorite was identified with the aid of QEMSCAN (Figure 8) in a single thin section as interparticle pore-filling constituent.

4.4 Fluid inclusions

Aqueous and oil fluid inclusions association (FIA) hosted in diagenetic constituents from the resedimented carbonates were analyzed (Figure 9). Three analyzed samples are from Well C1, and one from Well B1. The diagenetic phases analyzed are interparticle pore-filling and fracture-filling blocky dolomite, macrocrystalline calcite, prismatic quartz, saddle pore-filling, and matrix-replacive dolomite. The characteristics of the FIs in specific analyzed constituents can be summarized as follows.

Fluid inclusions from three FIAs in pore filling blocky dolomite at Well B1 (6 056.62 m) show relatively narrow *Th* variation within individual FIAs. Each assemblage presents three fluid inclusions analyses. The FIAs consisting of primary aqueous inclusions showed *Th* values between 51 and 62 °C, with salinity levels in individual assemblages ranging from 17 to 18 wt% NaCl equivalent (evaporitic-influenced).

Fluid inclusions from one FIA with only one secondary oil inclusion in diagenetic calcite (undetermined habit) at Well C1 (4 944.55 m) displayed orange-white fluorescence and *Th* of 102 °C.

Fluid inclusions from four FIAs in pore-filling prismatic quartz at Well B1 (6 056.62 m) show relatively large homogenization temperature (*Th*) variation within individual FIAs. Each assemblage contained between

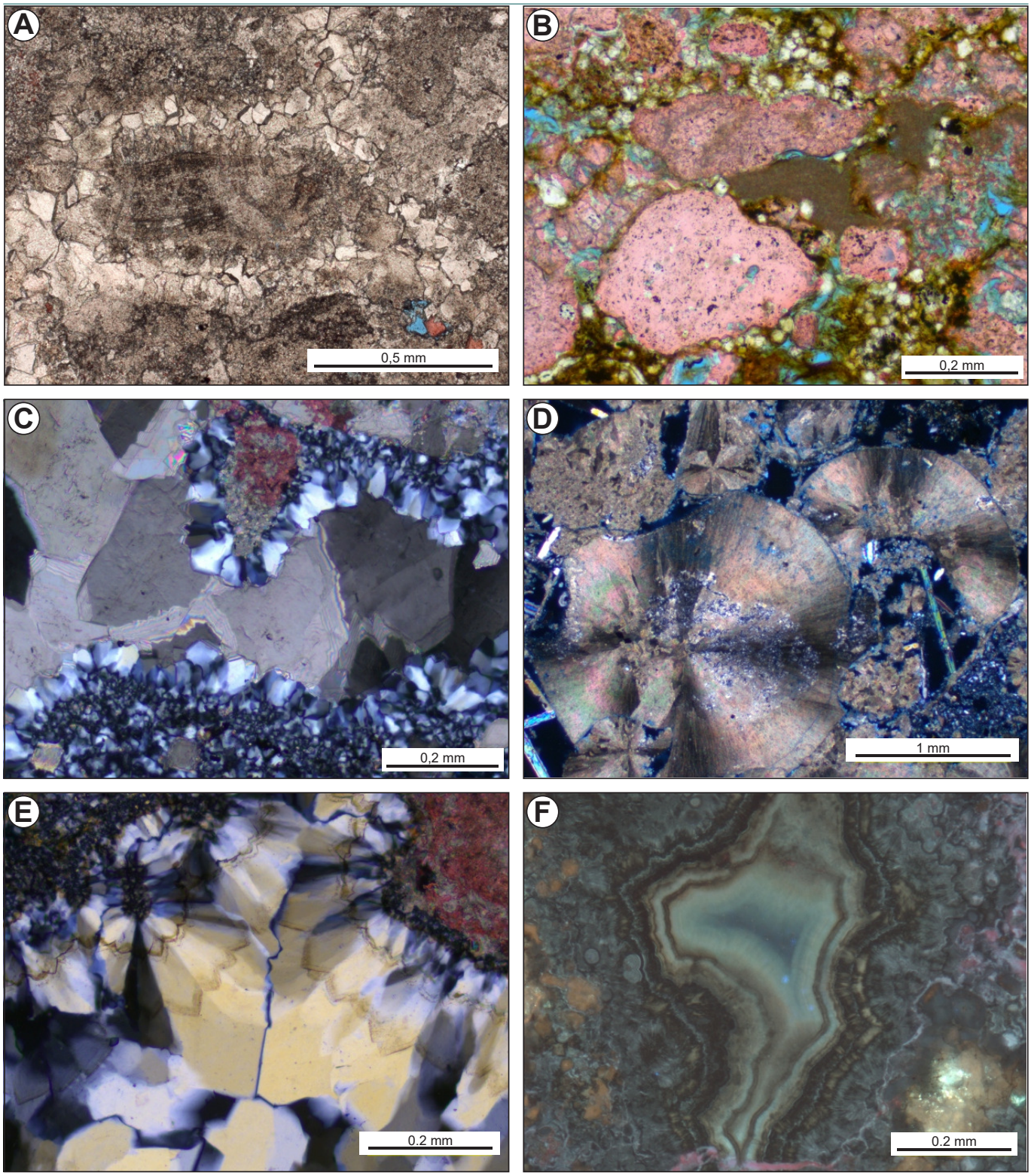

Figure 7 – Main diagenetic constituents of resedimented deposits. **(A)** Dolomitized carbonate intraclast and blocky dolomite filling interparticle porosity (//P). **(B)** Blocky dolomite replacing clay matrix (//P). **(C)** Saddle dolomite, precipitated upon macrocrystalline quartz, filling vuggy porosity (XP). **(D)** Spherulitic intraclasts replaced by pseudomorphic dolomite, partially dissolved (XP). **(E)** Microcrystalline quartz replacing the margins of the intraclasts, prismatic quartz rims covering the particles and macrocrystalline quartz filling interparticle porosity (XP). **(F)** Chalcedony lining vuggy pore in UV epifluorescence. The different silica growth phases are marked by oil inclusions. The center of the pore is filled with macrocrystalline quartz.

10 and 5 fluid inclusions. The FIA of primary gas condensate showed a Th_{vapor} of 81 to 90 °C, that coexists with biphasic aqueous inclusions with large vapor bubbles with a Th_{vapor} of 75 to 77 °C, for which salinity could not be measured. Additionally, the three FIAs of primary oil, presenting white, yellow, yellow-white and blue-green fluorescence colors, displayed a *Th* range of 47 to 100 °C, that coexists with aqueous

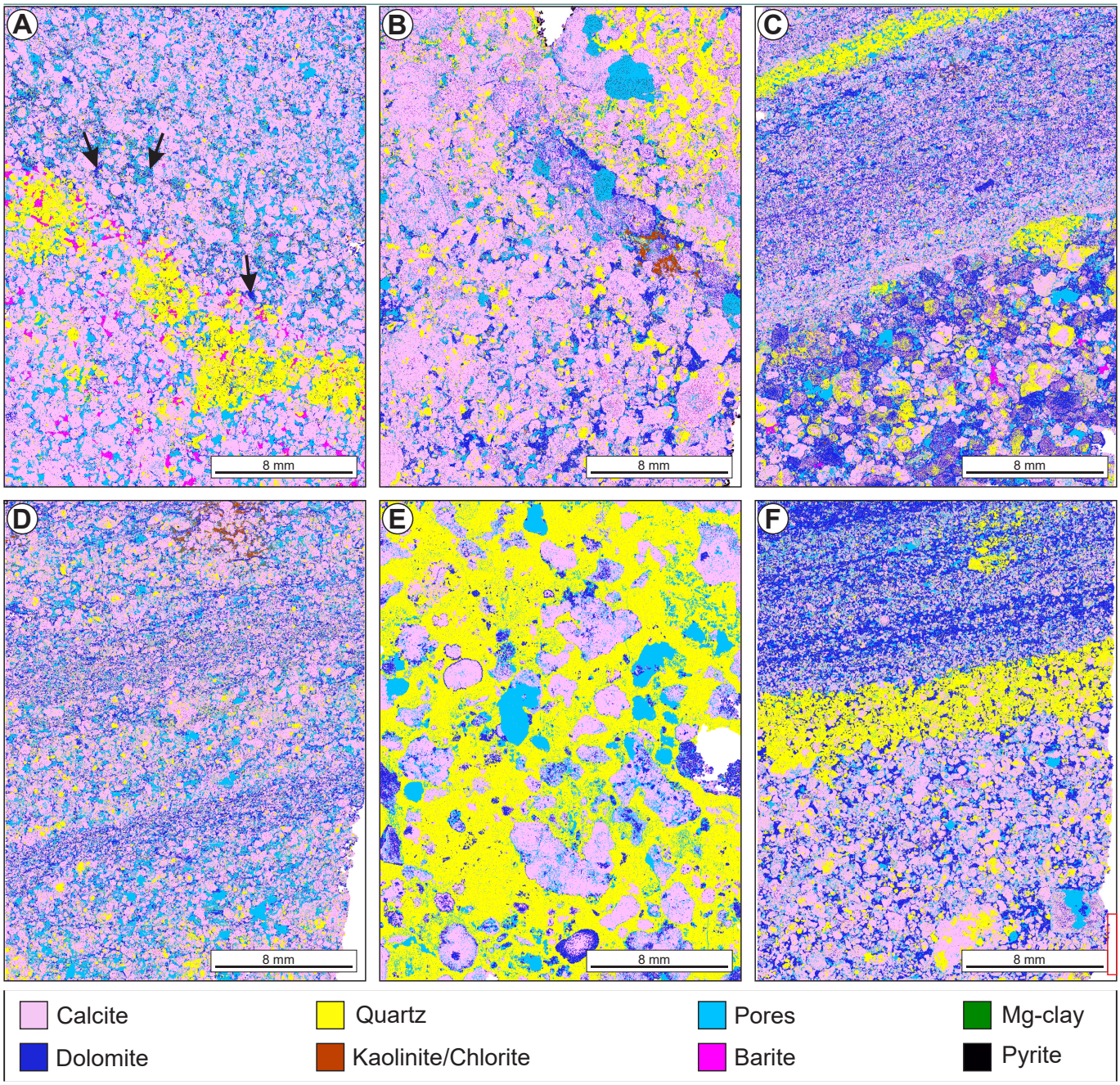

Figure 8 – QEMSCAN images showing structural, textural, and fabric features characteristic of the analyzed resedimented deposits. **(A)** Intraclastic calcarenite with an irregular silicified level. Remnants of laminated clay matrix replaced by dolomite (black arrows), and abundant barite filling interparticle porosity. **(B)** Rudaceous calcarenite partially cemented by quartz and dolomite. Kaolinite/chlorite replacing remnants of the clay matrix. **(C)** Contact between fine intraclastic-peloidal calcarenite and very coarse massive intraclastic calcarenite. Dolomite replacing the original matrix. The coarser portion is composed of carbonate intraclasts, with dolomite and quartz filling interparticle porosity. **(D)** Intraclastic-peloidal calcarenite with slightly dolomitized levels marking irregular lamination. Kaolinite/chlorite patches filling interparticle porosity. **(E)** Intensely silicified calcirudite, with several particles replaced by silica. Silica filling interparticle porosity. Moldic porosity formed by dissolution of carbonate intraclasts. **(F)** Laminated medium- to fine-grained calcarenite with interparticle porosity cemented by dolomite. A silicified level marks the contact between the two grain-size intervals.

inclusions that had a *Th* of 78 to 100 °C and salinity of 17 to 22 wt% (evaporitic-influenced).

Fluid inclusions from thirteen FIAs in pore-filling prismatic quartz at Well C1 (4 963.52, 4 944.55 and 4 977.66 m) show relatively large homogenization temperature (*Th*) variation within individual FIAs. Each assemblage contained between 13 and 1 fluid inclusions. The four FIAs of primary oil, presenting white and orange fluorescence colors, displayed a *Th* range of 54 to 143 °C. The two FIAs of pseudosecondary oil, presenting white and orange fluorescence colors, displayed a *Th* range of 75 to 124 °C. There are also three heterogeneous pseudosecondary FIAs presenting monophasic and biphasic aqueous

fluid inclusions that had a *Th* of 48 to 141 °C and salinity of 12 to 19 wt% (evaporitic-influenced). One pseudosecondary FIA consisting of aqueous inclusions showed *Th* values between 49 and 85 °C, with salinity levels in individual assemblages ranging from 16 to 21 wt% (evaporitic-influenced). Finally, one FIA of secondary oil with orange fluorescence colors, exhibited a *Th* of 71 °C; while two others secondary FIAs of aqueous inclusions had a *Th* of 97 to 150 °C and salinity of 14 wt% (evaporitic-influenced).

Fluid inclusions from four FIAs in replacive blocky dolomite at Well C1 (4 977.66 m) show relatively large *Th* variation within individual FIAs. Each assemblage contained between three and one fluid inclusions. The three FIAs consisting of primary oil inclusions showed *Th* values between 49 and 93 °C, presenting three fluorescence colors: white, yellow, and blue-white. The secondary FIA presents white fluorescence and *Th* of 52 °C.

Fluid inclusions from four FIAs in pore-filling saddle dolomite at Well C1 (4 963.52 m) show relatively large *Th* variation within individual FIAs. Each assemblage contained one fluid inclusion. The FIAs consisting of secondary oil inclusions showed *Th* values between 86 and 124 °C, presenting three fluorescence colors: white, yellow, and blue.

4.5 Porosity

The most common type of porosity in the resedimented deposits consists of intraparticle pores generated by partial dissolution of the carbonate intraclasts (34.8 % of total quantified pore volume), followed by interparticle (30.4 %), vuggy (20.3 %), and porosity from dissolution and shrinkage of clay and peloidal matrix (13.7 %). Interparticle porosity in the analyzed rocks is essentially primary. However, in some resedimented deposits with matrix, interparticle porosity was created by matrix dissolution, or is intercrystalline, among dolomite crystals that previously replaced the original clay matrix. Other minor pore types in these lithologies include vuggy, fracture and channel pores. Fracture, vuggy, and channel pores can be underestimated in petrographic analyses, because thin section preparation typically targets more massive areas of the rock, avoiding zones with fractures and larger vugs. In these cases, visualization of the sample in micro-CT images proves valuable for observing the pore system and interpreting permeability values (Figure 10).

4.6 Reservoir petrofacies

The resedimented deposits of the Barra Velha Formation were classified into ten reservoir petrofacies. The defined petrofacies reflect variations in the intensity of diagenetic processes, including cementation, replacement, and compaction. This section presents the main diagenetic and porosity characteristics of each petrofacies, with implications for reservoir quality.

IntracPor petrofacies correspond to resedimented "intraclastic" samples with more than 15 % of interparticle and non-fabric selective porosity (Table 3; Figure 10C and D). This petrofacies represents 11.89 % of the studied thin sections. The pore types in this petrofacies include interparticle, intraparticle, vuggy, and fracture pores. The average interparticle and non-fabric selective porosity is 17.43 %, while the average petrophysical porosity is 18.25 %. The average permeability is 0.385 μm^2 (390.6 mD).

Petrofacies with compaction as the main diagenetic modifier (IntracComp, IntracCompDol, and IntracCompPor) are represented by samples with low interparticle volume (< 35 %), abundance of concave-convex and sutured contacts, stylolites, grain fractures, and locally, pseudomatrix formed by the compaction of soft clay intraclasts. IntracComp and IntracCompDol petrofacies (Figure 10E and F), with less than 10 % of connected porosity, present predominantly framework dissolution intraparticle porosity (4.58 and 4.68 % respectively), with lower permeability values for IntracCompDol petrofacies. Among the defined reservoir petrofacies, IntracCompPor, with interparticle porosity between 10 and 15 %, presents the second-best average of permeability values. The main type of porosity in this petrofacies is interparticle, followed by intraparticle and vuggy porosity.

Dolomitized petrofacies (IntracDol and IntracDolPor) present more than 10 % of dolomite filling interstitial pores. IntracDolPor petrofacies (Figure 10G and H) shows between 10 and 15 % of interparticle and non-fabric selective porosity. The average porosity of the IntracDolPor petrofacies is 11.5 % and the maximum is 14 %, while the porosity values for the IntracDol petrofacies are 4.7 % in average and 9.5 % maximum. IntracDolPor presents the third highest average permeability values (avg. 0.269 7 μm^2 (273.27 mD); max. 1.579 μm^2 (1 600 mD)). This occurs where dolomite cementation creates a network of

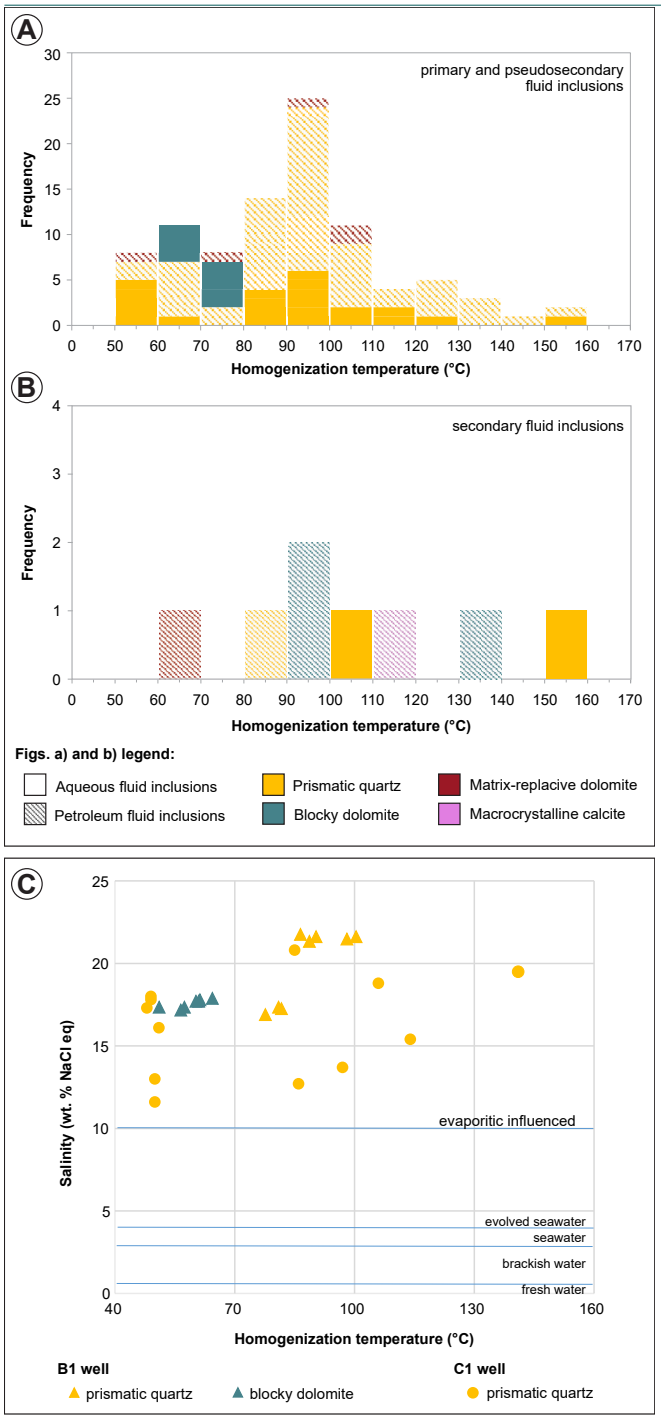

Figure 9 – Homogenization temperatures °C histograms of aqueous (solid colors) and petroleum (hatched colors) fluid inclusions hosted in diagenetic mineral phases from the Barra Velha Formation of Santos Basin, Brazil. **(A)** Primary and pseudo-secondary fluid inclusions. **(B)** Secondary fluid inclusions. **(C)** Homogenization temperature °C versus salinity (wt% NaCl eq.) cross plot for aqueous primary and pseudo-secondary fluid inclusions. Salinity varies in the range of 11.6 to 21.8 wt% NaCl eq.

intercrystalline pores, partially enlarged by slight dolomite dissolution.

Silicified petrofacies (IntracSil, IntracSilPor, and IntracDolSilPor) correspond to samples with interstitial silica, both filling the interparticle porosity and subordinately replacing clay matrix and peloids. In the IntracSil (Figure 10I and J) and IntracSilPor petrofacies, moldic and intraparticle pores prevail, commonly lined by silica cementation, which frequently leads to moderate porosity, but low permeability values. Locally, micro-CT reconstructions reveal fractured zones within the silicified petrofacies, which may act as conduits, significantly enhancing permeability in these intervals (Figure 10). IntracSil petrofacies presents 3 % average and 9.5 % maximum of connected porosity, and average permeability of 0.034 μm^2 (34.18 mD) (max. 0.495 μm^2 (501.9 mD)). IntracSilPor is the petrofacies with the smallest number of samples (only 4), with only two samples tested by RCAL, and therefore the permeability values may not be representative. The IntracDolSilPor petrofacies contain similar volumes of interparticle dolomite and silica, with an average connected porosity of 11.2 % and a maximum of 15 %. IntracDolSilPor petrofacies show average permeabilities of 0.039 2 μm^2 (39.7 mD) and a maximum of 0.063 2 μm^2 (64 mD).

5 Discussion

5.1 Depositional processes

The resedimented deposits in the pre-salt sag section of the Santos Basin are predominantly characterized by massive structures with moderate to good sorting, contrasting with typical features expected from high-energy depositional environments (Tucker & Wright, 2009). The dominant lack of depositional structures in these deposits provides important constraints on depositional mechanisms. While features of tractive processes characteristic of surface waves and currents, such as low-angle cross-stratification, hummocky cross-stratification, and current or wave ripples have been documented in specific areas (e.g., De Medeiros et al., 2024; Fragoso et al., 2023), the pre-salt resedimented deposit show dominantly massive structure. On the other hand, their redeposition by gravitational processes, as proposed by Barnett et al. (2021) and Wright (2022), seems to have been limited to few areas, as they are mostly distributed on top of structural highs, and not adjacent to them, and considering that subaerial exposure features are nearly absent in the section. The definition of the average and maximum water depth of the Aptian pre-salt lake is still a matter of considerable debate (e.g., Christ et al., 2025; Pietzsch et al., 2018, 2020; Wright, 2022; Wright & Barnett, 2017; Wright & Rodriguez, 2018).

Table 3 – Average and maximum values of the main types of pores described by petrography analysis (framework, interparticle, vuggy, total connected pores - without framework porosity, total petrographic porosity). The last 5 columns refer to RCAL data from plugs at the same depths of the studied thin sections.

Petrofacies	#	# (%)	Framework Pores		Interparticle Pores		Vugular Pores		Total Petrographic Connected Porosity		Petrographic Total Porosity		Petrophysical Porosity		# RCAL	Permeability μm^2 (mD)	
			Avg.	Max.	Avg.	Max.	Avg.	Max.	Avg.	Max.	Avg.	Max.	Avg.	Max.		Avg.	Max.
IntracCal	14.0	4.3	0.7	4.7	1.1	8.0	0.6	8.0	1.8	8.5	2.6	8.5	5.4	5.4	1.0		
IntracComp	24.0	7.3	4.6	23.0	2.5	6.3	1.1	7.5	5.0	9.5	9.6	26.3	13.2	23.6	13.0	47.0	373.1
IntracCompDol	26.0	7.9	4.7	8.0	2.6	8.0	0.6	6.5	4.1	9.0	8.8	13.7	13.4	19.6	18.0	11.2	61.5
IntracCompPor	16.0	4.9	3.9	10.0	7.8	14.0	2.1	8.0	11.4	14.0	15.2	20.0	17.0	25.3	12.0	322.3	1700.0
IntracDol	95.0	29.0	3.7	15.0	1.8	8.7	0.8	7.0	4.7	9.5	8.3	17.5	14.3	31.7	61.0	23.6	716.1
IntracDolPor	42.0	12.8	3.2	6.5	5.3	13.4	3.5	10.0	11.5	14.0	14.7	20.0	15.8	22.2	27.0	273.3	1600.0
IntracDolSilPor	9.0	2.7	3.8	7.0	5.3	10.0	5.1	10.0	11.2	14.0	15.1	17.0	14.8	19.4	6.0	39.8	64.0
IntracPor	39.0	11.9	3.7	12.0	9.1	25.0	5.9	20.0	17.4	27.0	21.2	30.5	18.2	32.6	29.0	390.6	2750.0
IntracSil	59.0	18.0	4.8	16.0	0.8	8.5	1.9	9.0	3.0	9.5	7.8	20.0	9.8	25.4	28.0	35.2	501.9
IntracSilPor	4.0	1.2	5.1	8.0	1.9	3.0	9.9	13.0	11.8	13.5	16.9	19.5	9.1	14.4	2.0	0.6	1.1

The widespread distribution of these deposits across the Santos and Campos basins in the eastern Brazilian margin (e.g., Barnett et al., 2021; Carramal et al., 2022; Carvalho et al., 2022; Herlinger et al., 2017; Lima & De Ros, 2019; Wright & Barnett, 2017), and Kwanza Basin in Angola (e.g., Sabato Ceraldi & Green, 2016; Saller et al., 2016) further suggests a regionally significant process rather than localized sedimentary events (Altenhofen et al., 2024, 2026). This distribution and the depositional structure of most of the pre-salt resedimented deposits have stimulated Altenhofen et al. (2024, 2026) to propose internal waves of the chemocline of the pre-salt stratified (meromictic) alkaline lacustrine system as the main mechanism for their generation. Internal waves have been identified as important agents of resedimentation in lacustrine and marine environments (Apel et al., 2007; Bádenas et al., 2012; Pomar et al., 2012; Preusse et al., 2010), and provide a viable mechanism to account for the recurrent intercalation of resedimented and in situ deposits and their widespread distribution across the Santos, Campos, and Kwanza basins (Altenhofen et al., 2024, 2026).

5.2 Paragenetic evolution

The diagenetic processes of resedimented deposits from the sag section of the Santos Basin are the main control on their reservoir quality. The integrated approach, combining systematic petrography, fluid inclusion microthermometry, micro-computed tomography, and reservoir petrofacies analysis, contributed to understanding the diagenetic evolution of these rocks, and their relations with reservoir quality and basin evolution.

Dolomite and silica cementation, along with compaction, are the main diagenetic processes impacting the reservoir quality of the pre-salt resedimented reservoirs. Both dolomite and silica precipitation occurred under diverse conditions, as suggested by their paragenetic relations and distribution patterns. The presence of heterogeneous aqueous fluid inclusions (liquid and liquid + vapor) entrapped at low temperatures in an evaporative context is indicative of eodiagenesis. The wide range of homogenization temperatures supports the occurrence of multiple events of dolomite and silica precipitation (Figure 11A) and indicates post-trapping stretching re-equilibration processes (Goldstein, 2001; Goldstein & Reynolds, 1994) in some fluid inclusion assemblages (FIAs), which re-equilibrated the original entrapment temperatures to a gradation of higher values. For FIAs with clear evidence of stretching, only the minimal *Th* mode of aqueous FIAs was considered representative of the original entrapment conditions.

Dolomite commonly occurs as blocky and saddle habits replacing and cementing the resedimented deposits. Dolomite precipitation in alkaline lacustrine deposits is well documented in the literature (Guo et al., 2023; Hirst, 1995; Last, 1990; Tosca & Tutolo, 2023) and is often interpreted as the result of alteration of magnesium-rich clay minerals (Li et al., 2023; Tutolo & Tosca, 2018). Homogenization temperatures measured in primary aqueous inclusions hosted by blocky dolomite cement from Well B1 showed a narrow range between 51 and 62 °C within an evaporitic-influenced setting, indicating precipitation during the initial stages of burial diagenesis (Immenhauser, 2021). Paragenetic relationships suggest that blocky dolomite precipitated before compaction (Figure 11B), in some samples, and post-compaction (Figure 11C), in others. Replacive blocky dolomite, occurring as a replacement of intraclasts and clay matrix, contains oil inclusions with *Th* values between 49 and 93 °C, indicating replacement processes during both eodiagenesis and mesodiagenesis.

Late saddle dolomite precipitated during deeper burial diagenesis. These crystals are often filling fractures or vuggy pores in the resedimented deposits, also suggesting precipitation from late fluids, marked by secondary oil FIAs with minimal *Th* of 86 and 124 °C. The paragenetic relations of saddle dolomite, post-dating compaction and other interparticle pore-filling phases, reinforces its origin under mesodiagenetic or hydrothermal conditions (Machel, 1987; Spötl & Pitman, 1998). Lima et al. (2020) associated the presence of saddle dolomite, with other minerals such as macrocrystalline calcite, mega-quartz, Sr-barite, celestine, fluorite, dickite, sphalerite, galena, and other metallic sulfides, to a hydrothermal system with some analogy to carbonate-hosted Pb-Zn Mississippi Valley (MVT) and Irish-type ore deposits.

The larger amount of macrocrystalline calcite cement in Well A2 may be related to a particular primary composition of the Barra Velha Formation basal section. These hybrid arenites contain abundant volcanic clasts, which may be one of the sources of Ca for the abundant precipitation of interparticle calcite in these rocks. The hybrid rocks exhibit intense compaction, characterized by tight grain packing and abundant

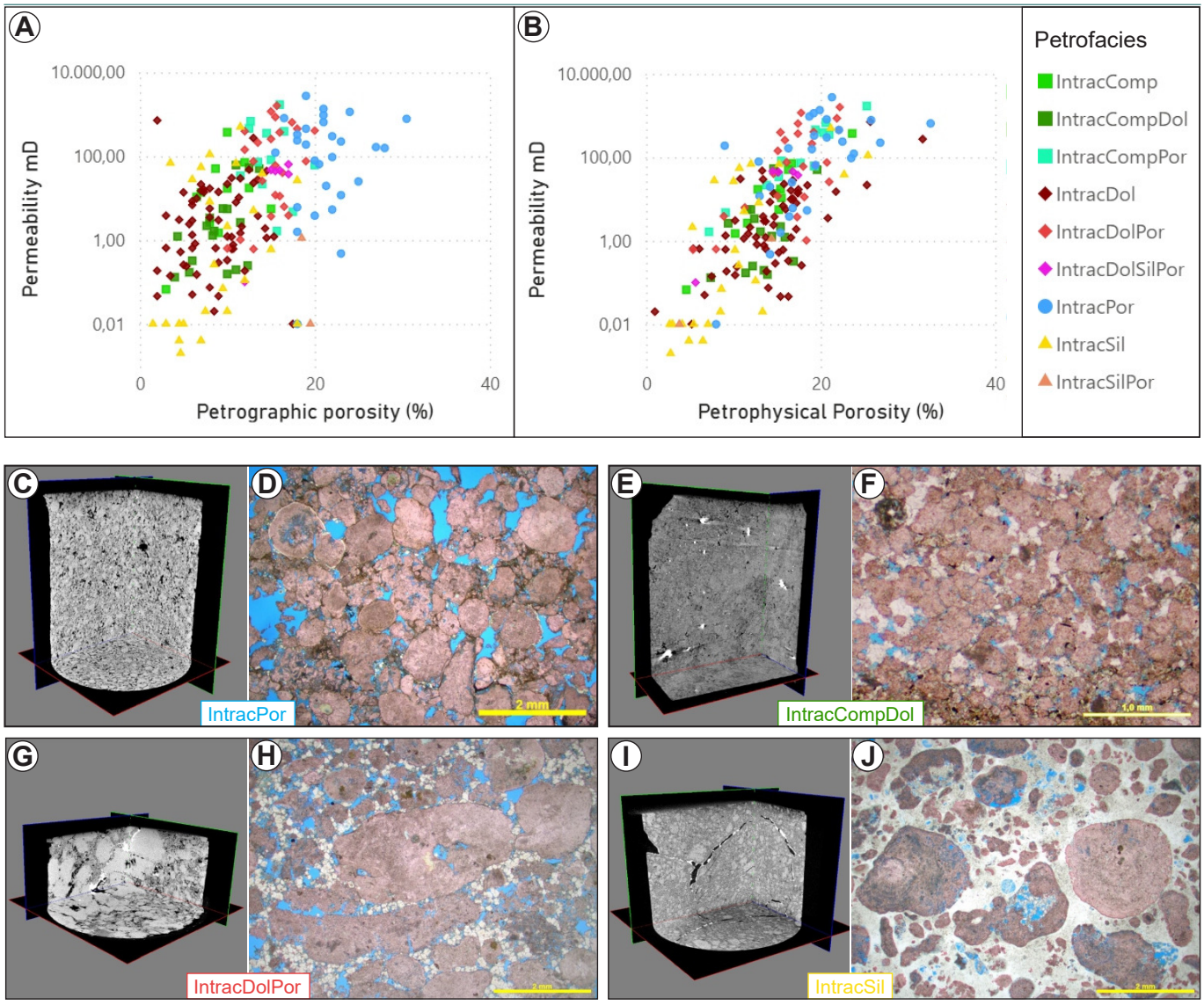

Figure 10 – Integration of petrographic, RCAL, and micro-CT data for the main petrofacies. **(A)** Cross-plot of porosity observed in petrographic analysis vs. RCAL permeability. **(B)** Cross-plot of RCAL porosity and permeability. **(C)** 3D micro-CT reconstruction and **(D)** thin section image corresponding to the IntracPor petrofacies (//P). **(E)** and **(F)** IntracCompDol petrofacies (//P). **(G)** and **(H)** IntracDolPorl petrofacies (//P). **(I)** and **(J)** IntracSil petrofacies (//P).

concave–convex and sutured interparticle contacts, indicative of dissolution by chemical compaction. Calcite cementation likely occurred after compaction, obliterating the interparticle porosity of these rocks (Figure 11G). Calcite also occurs in smaller volumes as an eodiagenetic constituent, replacing the clay envelopes of ooids and covering the intraclasts as rims of blocky crystals. These rims are commonly dissolved or replaced during later diagenetic evolution.

At least two phases of silicification occurred during the early diagenetic stage, and another silicification phase took place during late diagenesis. The earliest and most abundant phase occurs as interparticle pore-filling silica cement. This phase was associated with the release of Si from the dissolution of abundant magnesian clays of the in situ associated deposits. This initial and most significant silicification process preceded hydrocarbon charge and the arrival of organic acids (Christ et al., 2025). The dissolution of Mg-clays was interpreted as the main source of Mg^{2+} and Si^{4+} (aq·) for the silicification and dolomitization of pre-salt deposits (Tosca & Wright, 2015), since Mg-clays are known to be chemically labile and prone to rapid destabilization and dissolution during diagenesis (Deocampo, 2015; Tosca & Masterson, 2014; Tosca & Wright, 2015).

The eodiagenetic precipitation of silica is favored over dolomite precipitation by a decrease in Mg^{2+} concentration or a slight decrease in pH. These conditions promoted early cementation of the resedimented deposits by microcrystalline silica prior to compaction, thereby preserving significant interparticle volume

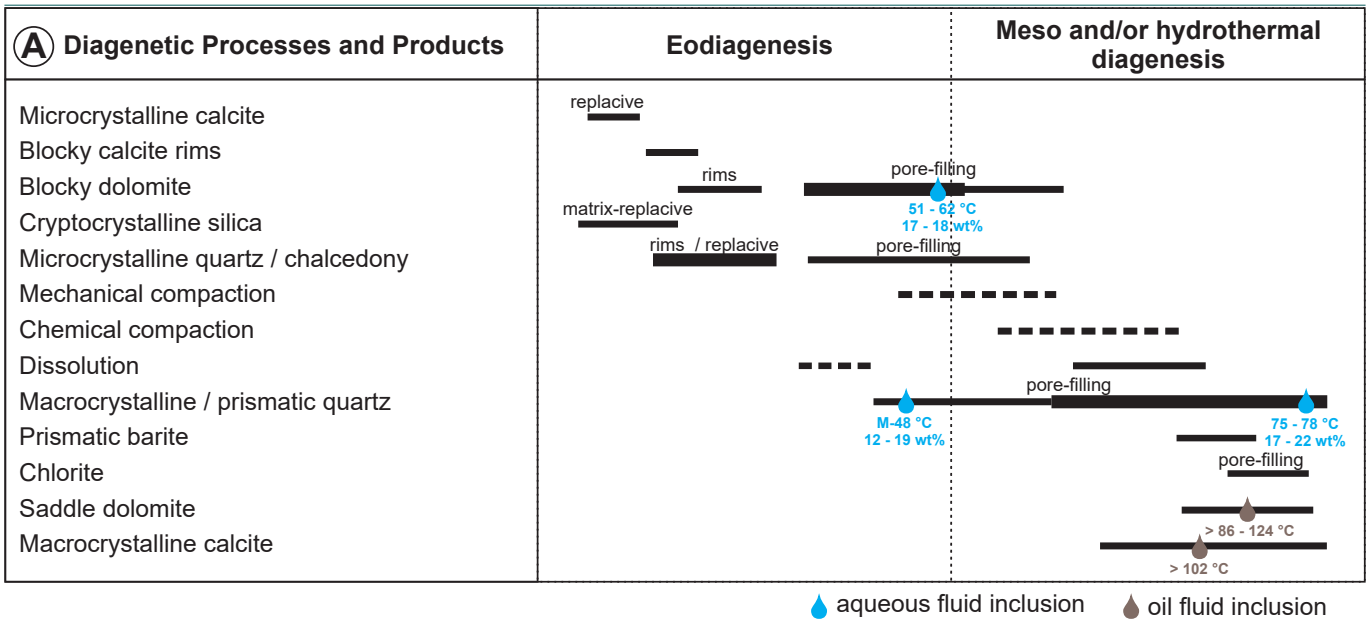

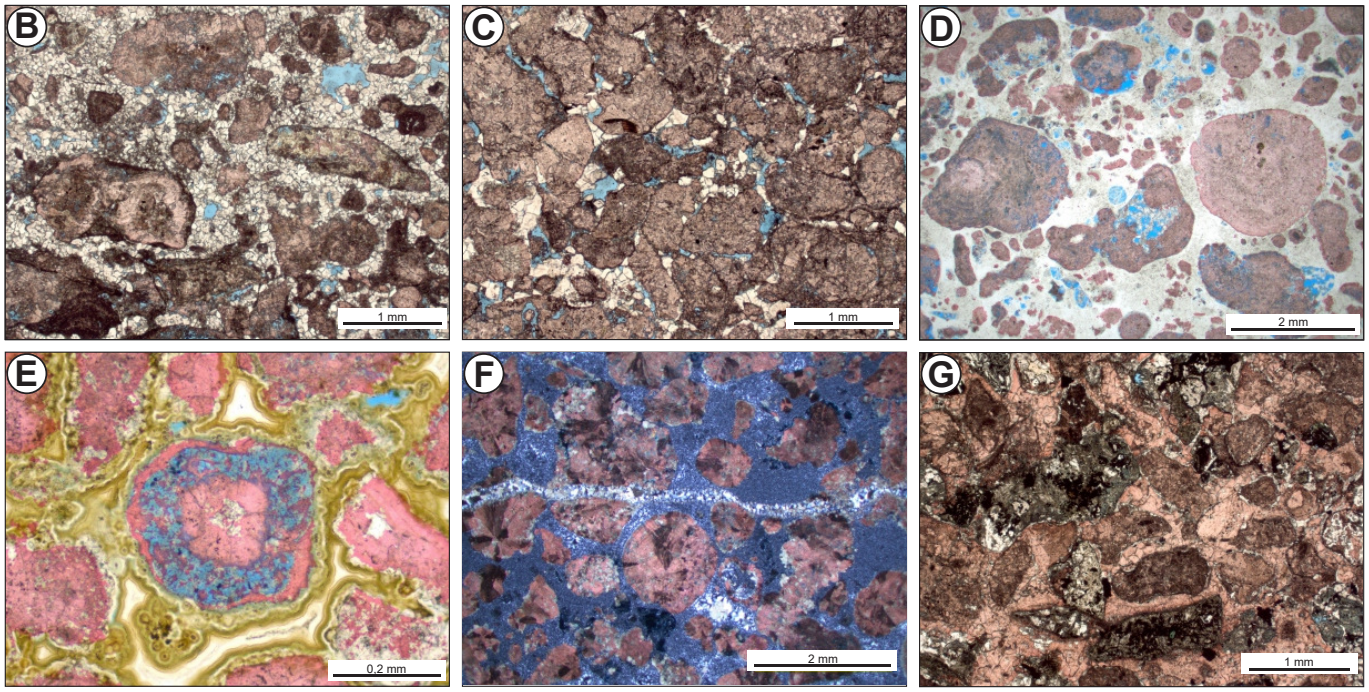

Figure 11 – **(A)** Paragenetic sequence of the studied Barra Velha Formation resedimented deposits. The thickness of the lines corresponds to the intensity or abundance of the processes and products. Blue drops represent aqueous fluid inclusion microthermometry temperature values for original mineral precipitation conditions, and brown drops represent oil fluid inclusions. **(B)** Pre-compaction interparticle blocky dolomite (//P). **(C)** Syn-compaction and post-compaction interparticle blocky dolomite (//P). **(D)** Eodiagenetic, pre-compaction interparticle microcrystalline quartz cementation (//P). **(E)** Pre-compaction interparticle oil-impregnated chalcedony cementation (//P). **(F)** Prismatic quartz filling fracture in rock previously cemented by microcrystalline quartz (XP). **(G)** Macrocrystalline calcite filling the interparticle porosity in Well A2 (//P).

(Figure 11D). According to Wright & Barnett (2015), early silica nodules and layers in the Barra Velha Formation would have originated from the precipitation of silica gels during freshening episodes of the lake waters and a decrease of pH. However, given the large extent of the pre-salt lake system, encompassing several South Atlantic basins, it is unlikely that the input of meteoric fluids into the basin alone could have caused the frequent early silicification episodes observed throughout the lacustrine system (Schrank et al., 2024). The coexistence of gas condensate, light oil, and evaporitic-influenced aqueous fluids in prismatic quartz suggests an alternative to Wright & Barnett's (2015) freshening hypothesis. Rather than precipitation from gels during freshening episodes, fluid inclusion data indicate eodiagenetic silica precipitation (replacement and cementation) under sustained evaporitic lake conditions, without drastic changes in water chemistry.

A second silicification style that occurred during the early diagenetic stage may be linked to the shallow percolation of hydrothermal fluids prior to the deposition of the thick salt section. Schmidt et al. (2025) identified an early hydrothermal, atypical petroleum system (sensu Magoon & Dow, 1994) in rocks of the Barra Velha Formation, based on the occurrence of fluid inclusions containing condensate gas coexisting with light oil (heterogeneous trapping). Guzzo et al. (2018) also previously described an atypical petroleum system in the Barra Velha Formation, evidenced by the presence of a wide range of fluid inclusion homogenization temperatures (50 to 160 °C) hosted in early diagenetic cements, along with molecular indicators of oil biodegradation in pre-salt oils. Abundant oil inclusions and some heterogeneous aqueous pseudosecondary inclusions in early cements are common at certain analyzed depths, particularly within eodiagenetic pore-filling prismatic quartz and chalcedony (Figure 11E). If the generation of this early oil charge is indeed related to a hydrothermal system, its paragenetic relations (occurring within pre-compaction cements) support the interpretations of Guzzo et al. (2018) and Schmidt et al. (2025) of an early-stage hydrothermal alteration of the pre-salt rocks. Hydrothermal systems can also promote silicification through the formation of organic acids produced by the thermal degradation of organic matter (Tosca & Wright, 2015).

There is no clear correlation between the salinity and temperature of fluid inclusions (Figure 9C). Salinities are less variable in Well B1 compared to Well C1. All salinity values above 10 wt% (NaCl eq.) indicate fluids influenced by highly evaporitic conditions. Salinity between 15 to 10 wt% (NaCl eq.) may indicate mixing between saline connate fluids and pulses of brackish juvenile fluids, as suggested by Schmidt et al. (2025). These brackish juvenile fluids likely percolated laterally and vertically through the reservoir interval carrying droplets of hydrothermal oil. Based on associated oil and aqueous fluid inclusion assemblages, Schmidt et al. (2025) identified multiple episodes of petroleum generation-migration in some Barra Velha fields.

Late-stage silica precipitation is characterized predominantly by macrocrystalline, prismatic, and drusy quartz. Numerous studies have associated such coarse-crystalline quartz, which typically occurs filling non-selective porosity (fractures, vugs, and channels), with a late hydrothermal origin in the pre-salt rocks (Basso et al., 2023; Fernández-Ibáñez, Nolting, et al., 2022; Lapponi et al., 2019; Lima et al., 2020; Sartorato et al., 2020; Teboul et al., 2019; Wennberg et al., 2021). In the studied resedimented deposits, coarse crystalline quartz is found filling fractures (Figure 11F), channel pores, and vugs, mainly in Well C1. This process likely developed more brittle mechanical characteristics, making the rock more susceptible to fracturing. The early fracturing subsequently favored more intense fluid circulation during late diagenesis. Furthermore, the dissolution of carbonates and precipitation of silica were facilitated by the inverse solubility relationship between carbonates and silica under decreasing pH conditions associated with the inflow of more dilute hydrothermal fluids (Poros et al., 2017).

The diagenetic evolution of the wells studied in the fields A, B, and C reveals a broadly comparable paragenetic framework with intense dolomitization and silicification. Distinct diagenetic pathways occur in some wells due to particular depositional characteristics (presence of clay and peloids with magnesian matrix, or volcanic fragments) or due to the structural framework in which the well is located (structural lows or highs associated with major faults).

The A Field is characterized by multi-phase dolomitization, which constitutes the dominant diagenetic mechanism. Early pseudomorphic, microcrystalline, and lamellar dolomite preserved original depositional fabrics, while saddle dolomite filled pores during mesodiagenesis. Localized calcite cementation in hybrid arenites at the base of Well A2 resulted in near-complete occlusion of primary porosity, forming diagenetic compartmentalization in resedimented reservoirs.

In the B Field, abundant Mg-clay matrix is preserved in Well B1. Dolomitization is pervasive, occurring predominantly as blocky and saddle dolomite and exerts a moderate impact on pore network modification. Silicification is subordinate relative to the other fields and does not significantly overprint primary textures. Consequently, the reservoir quality in B Field is strongly controlled by the interplay between matrix preservation and restrained diagenetic replacement.

The C Field exhibits the most complex and intense diagenetic overprint among the three areas. Silicification is the dominant process and occurs as a multistage sequence ranging from cryptocrystalline and chalcedonic replacement to late euhedral quartz precipitation. The presence of dawsonite, coupled with

fabric-destructive silica phases, suggests episodic hydrothermal input. The resedimented deposits prevail in the C1 well. Despite extensive silica replacement, porosity remains locally preserved or enhanced through dissolution and fracturing, resulting in a complex but effective reservoir system.

Although all three fields share an initial mineralogical and depositional framework, their diagenetic divergence significantly influenced petrofacies evolution and reservoir performance which are discussed in sequence. The B Field shows that the preservation of primary matrix content mixed with resedimented deposits controlled reservoir behavior. The C Field contains intensely replaced rocks dominated by hydrothermal silica and late-stage mineral precipitation. The A field records a dolomite predominance with development of well-connected intercrystalline pore networks. These contrasts emphasize the role of structural positioning and lithological heterogeneity in determining reservoir quality in the pre-salt.

5.3 Diagenesis and reservoir quality

The primary porosity in the analyzed resedimented deposits is interparticle, as in many examples of the pre-salt carbonate rocks (Herlinger et al., 2017). Preserved porosity in pre-salt resedimented reservoirs is controlled far more by diagenetic evolution than by depositional texture. Unlike the in situ rocks of the Barra Velha Formation, where porosity is mainly secondary, generated by dissolution of the Mg-clay matrix (Schrank et al., 2024), the diagenetic processes had a mostly negative impact on porosity of the resedimented deposits. The scatter plots in Figure 12 demonstrate the impact of diagenetic constituents on porosity for the studied resedimented deposits. It is observed that the calcite-cemented rocks present low total porosity values. Dolomite shows no clear control over porosity loss. Silica displays a more evident negative correlation with porosity than dolomite in the analyzed thin sections.

The flowchart in Figure 13 illustrates the diagenetic pathways of the analyzed resedimented deposits, both with and without depositional matrix, and their classification into distinct reservoir petrofacies. This classification is critical for understanding reservoir quality distribution within the resedimented deposits of the Barra Velha Formation, as each petrofacies represents a combination of depositional and diagenetic features that control fluid flow and hydrocarbon storage.

Some Barra Velha resedimented deposits were deposited with a magnesian clay matrix. This was promoted by incomplete winnowing of the syngenetic Mg-clay matrix during reworking of the in situ deposits, allowing the deposition of clay laminations intercalated among the intraclastic deposits. The scarcity of argillaceous intraclasts was interpreted by Altenhofen et al. (2026) as a product of the low cohesion of the Mg-clay matrix due to the lack of microbial colonization on the clay deposits. Compaction of the few clay intraclasts formed a clay pseudomatrix filling interparticle porosity.

In resedimented deposits with matrix, the destabilization of the magnesian clay minerals released ions that promoted widespread dolomitization in these rocks. The replacement of the argillaceous matrix by microcrystalline and blocky dolomite during early diagenesis, prevented stronger compaction. Silica also replaced the argillaceous matrix where and/or when pH decreased. The eodiagenetic environment, rich in HCO_3^-, Ca^{2+}, Si^{4+}, and Mg^{2+} ions, promoted extensive pre-compaction silica and dolomite cementation. Both the interparticle silica and dolomite cements nucleated along the surfaces of the carbonate particles and grew toward the pore centers (Schrank et al., 2024).

Eodiagenetic calcite precipitation occurred mostly as blocky crystals on the surfaces of the intraclasts. During mesodiagenesis, the infilling of interparticle porosity by macrocrystalline calcite, particularly in Well A2, may have been favored by proximity to the volcanic basement rocks, which the alteration may have supplied Ca^{2+} ions for such abundant calcite precipitation.

The porous IntracPor petrofacies ($\phi > 15\,\%$) present pore systems consisting essentially of interparticle pores. However, some resedimented deposits may present more complex pore systems including vugs, fractures, and channels. Early interparticle dolomite and silica cementation stabilized the framework of these rocks but obliterated their primary interparticle porosity. The subsequent preferential dissolution of the calcite particles created intraparticle and moldic porosity. In silicified rocks, dissolution formed poorly connected moldic porosity resulted in low permeability values. In rocks cemented by dolomite, the dissolution of the particles locally formed vuggy porosity, owing to their intercrystalline porosity among the dolomite crystals.

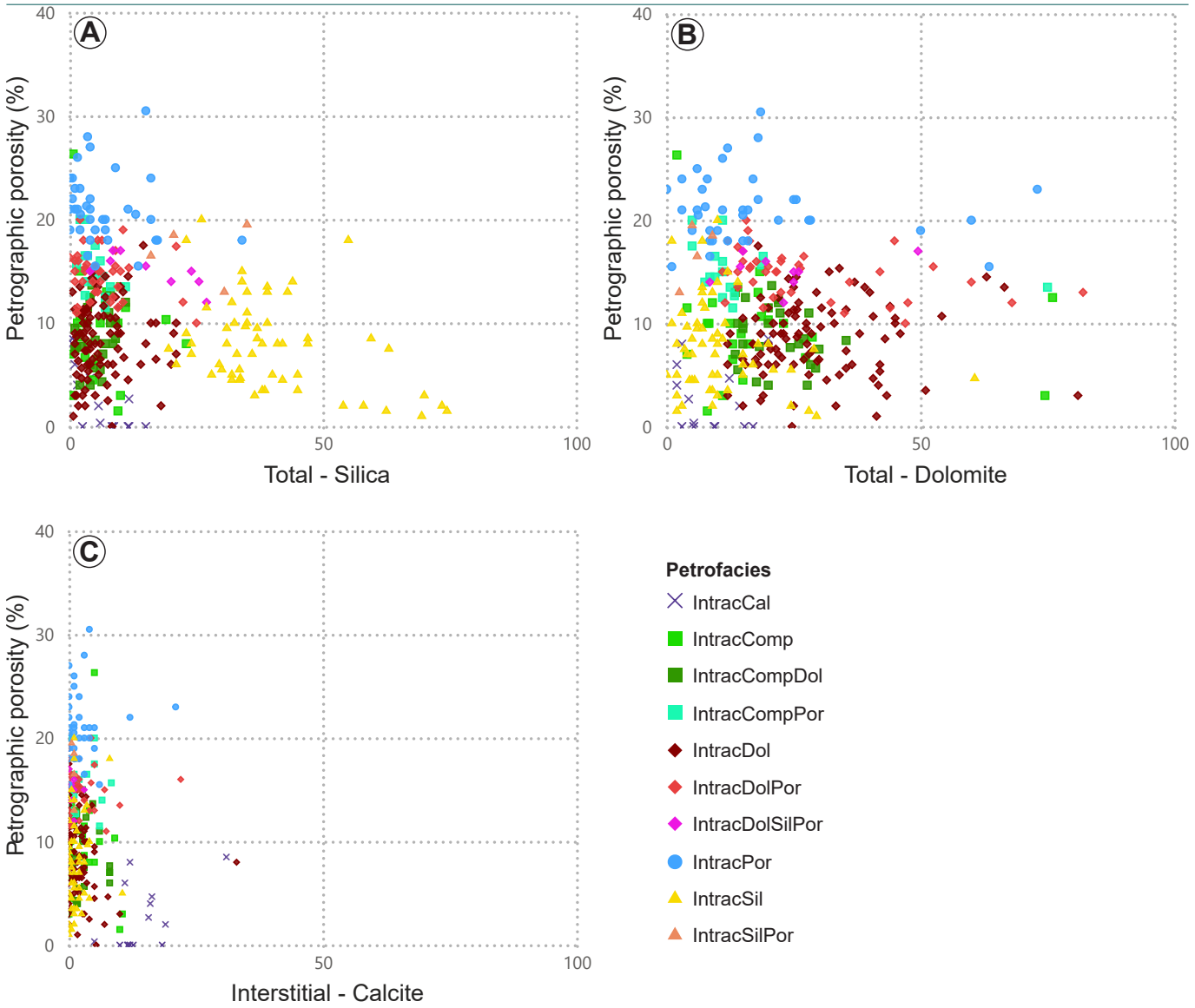

Figure 12 – Cross-plots showing the relation of the main diagenetic constituents **(A)** silica, **(B)** dolomite, **(C)** calcite cement with porosity.

The compacted IntracCompPor petrofacies that retain between 10 and 15 % of porosity represent the group with the second highest permeability values. A plausible explanation is that in these compacted rocks lacking cementation, the interparticle porosity was not occluded; instead, compaction mostly increased the tortuosity of the pore network (Budd, 2002). The pore systems of the IntraComp and IntracCompDol petrofacies (with pore volume below 10 %) are represented mainly by secondary intraparticle pores, formed by dissolution and fracturing of the carbonate particles.

The resedimented deposits of the Barra Velha Formation were particularly more susceptible to compaction than the in situ deposits, whose more stable framework prevented more intense compaction processes (Rossoni et al., 2024; Schrank et al., 2024). Partial cementation by calcite, dolomite, or quartz, either as rims or as discrete crystals, commonly enabled the preservation of interparticle porosity by preventing intense compaction (e.g., Morad et al., 2012).

Petrofacies affected mainly by interparticle cementation or early replacement of the clay matrix by dolomite or silica, show decreased permeability due to isolation of the pores (Budd, 2002). Where intense interparticle pore reduction by dolomite cementation occurs (< 10 % porosity), a strong impact on throat size relative to pore size is observed, as described by Herlinger et al. (2023).

Silica cementation resulted in petrofacies that, even with moderate interparticle pore volumes between 10 and 15 %, show low to moderate permeability values. Some exceptions occur where vuggy pores

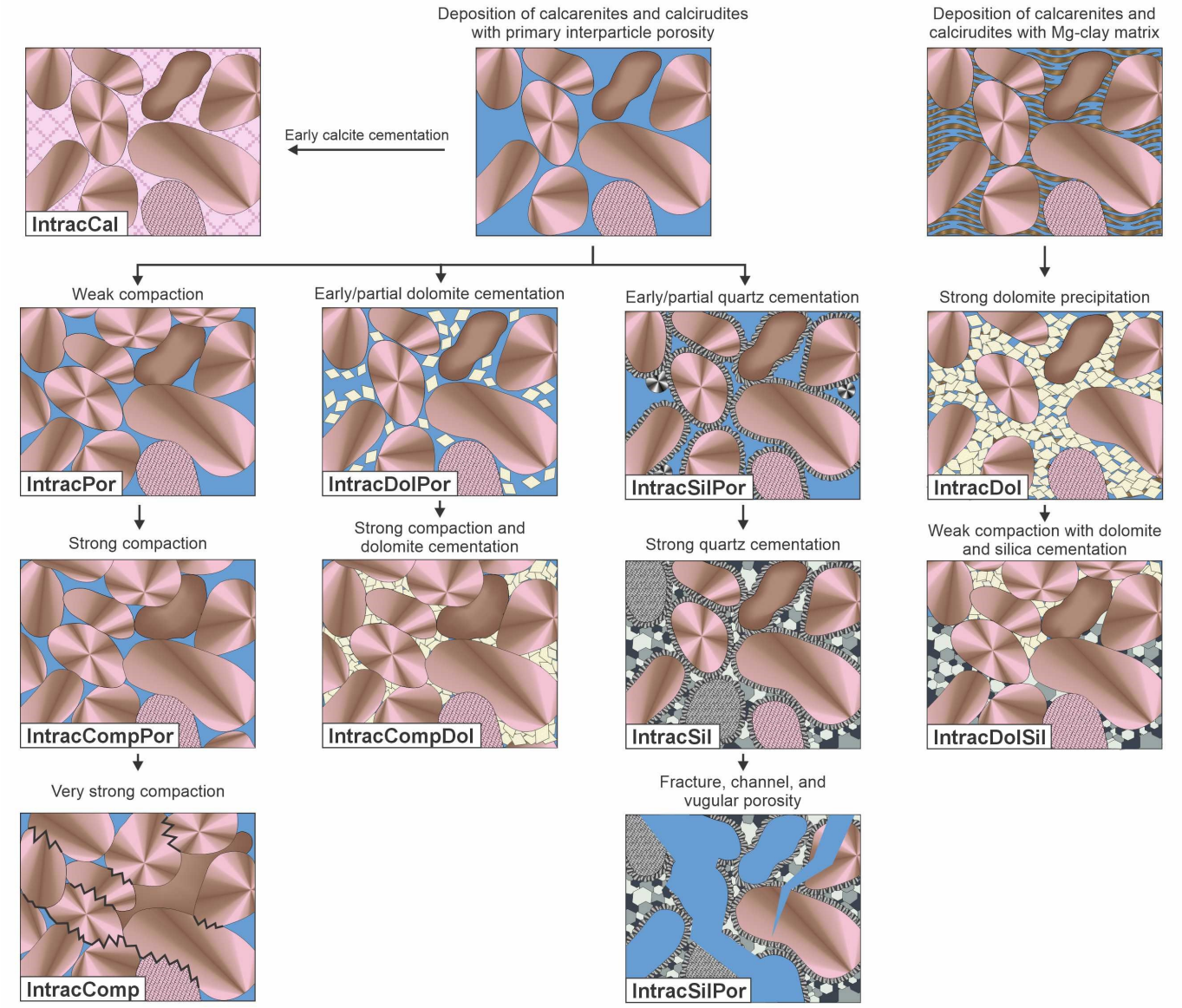

Figure 13 – Schematic diagenetic evolution of the resedimented deposits and corresponding potential reservoir petrofacies.

associated with fracturing connected the moldic and intraparticle porosity, which formed silicified rocks with well-connected pore systems. Early cementation and replacement by silica made these rocks more brittle and susceptible to fracturing. Fracturing created areas with significantly enhanced permeability. Where associated with ascending corrosive fluids, channels or vuggy pores formed. However, the occurrence of vuggy pores totally cemented by drusiform silica is common in these rocks, indicating more than one phase of silicification and the complex impact of the silicification processes on the quality of the pre-salt reservoirs.

6 Conclusions

- Through a multi-methodological approach, we successfully characterized reservoir petrofacies with distinct evolutionary pathways and differential quality within the resedimented deposits of the pre-salt Aptian Barra Velha Formation in the Santos Basin. The reservoir petrofacies methodology is crucial for the exploration and development of heterogeneous pre-salt reservoirs, despite the relatively simple primary textural and mineralogical composition of the resedimented pre-salt deposits.
- Dolomite and silica precipitated in a multiphase pattern, as evidenced by their paragenetic relations and distribution. Multiple dolomite and silica precipitation events are also supported by the presence of fluid inclusions with heterogeneous trapping and a wide range of homogenization temperatures.

- Blocky dolomite precipitated prior to compaction in some samples and post-compaction in others. Late saddle dolomite precipitated during deeper burial diagenesis.
- At least two phases of silicification occurred during the eodiagenetic stage, with an additional silicification phase occurring during late burial diagenesis.
- The relative timing between compaction and the precipitation of eodiagenetic dolomite, silica, or calcite determines the reservoir quality of the resedimented Barra Velha Formation deposits. Mesodiagenetic or late hydrothermal processes exerted less influence on the porosity evolution of the resedimented deposits.
- Resedimented deposits were more susceptible to compaction than the in situ deposits, which show better reservoir potential in some areas, owing to a relatively more stable crystalline framework.
- These insights are key to predicting reservoir quality and optimizing the development strategies for pre-salt accumulations, as well as improving the understanding of the diagenetic evolution of resedimented lacustrine carbonates in general.

Acknowledgements

The authors thank the Graduate Program in Geosciences at the Federal University of Rio Grande do Sul for support during the doctoral research. We also thank the Institute of Petroleum and Natural Resources (IPR) at the Pontifical Catholic University of Rio Grande do Sul (PUCRS) and Equinor Brazil for providing financial support and well data. Lastly, we thank Executive Editor Giovanna Della Porta, Associate Editor Arnauld Gallois, and the reviewers for their valuable contributions to a previous version of the manuscript.

Data and code availability

The data are subject to confidentiality restrictions imposed by the company consortium and therefore are not publicly available. Access may be granted upon request and with permission of the consortium.

Supplementary materials

Supplementary material to this paper can be found with the online version at doi:10.57035/journals/sdk.2026.e41.2335

Conflict of interest statement

The authors declare that they have no conflicts of interest in relation to the contents of this work.

Artificial intelligence use statement

All research, analysis, writing, and editing were performed without generative AI assistance.

Funding

The first author acknowledges the financial support from the Human Resources Program of the Brazilian National Agency for Petroleum, Natural Gas and Biofuels (PRH/ANP – PRH14/Geosciences UFRGS), funded by resources from the investment of qualified oil companies under the R&D Clause of ANP Resolution No. 50/2015, and from the São Paulo Research Foundation (FAPESP), grant No. 2024/10540-7. We acknowledge the funding from Equinor Brazil through ANP R&D levy regulation (grant number 21761-2).

Citing this Research Article

To cite this paper use the following information:

Authors

Mariane Cristina Trombetta, Sabrina Danni Altenhofen, Jaques Soares Schmidt, William da Silveira Freitas, Rosalia Barili, Amanda Goulart Rodrigues, and Luiz Fernando De Ros

Title

Diagenetic evolution and reservoir quality of Aptian lacustrine resedimented deposits from the Santos Basin, Brazilian pre-salt

Short Title

Diagenesis of resedimented pre-salt deposits

Publishing Information

Publication: Sedimentologika
Volume: 4
Issue: 1
Year: 2026
DOI: 10.57035/journals/sdk.2026.e41.2335
Language: en

References

Agência Nacional do Petróleo. (2025a). *GeoMapsANP*. Agência Nacional do Petróleo. Map | ANP. https://geomaps.anp.gov.br/

Agência Nacional do Petróleo. (2025b). *Production bulletin – Pre-salt data: Interactive production dashboard*.

Altenhofen, S. D., Rodrigues, A. G., Borghi, L., & De Ros, L. F. (2024). Dynamic re-sedimentation of lacustrine carbonates in the Búzios Field, pre-salt section of Santos Basin, Brazil. *Journal of South American Earth Sciences*, *138*, 104863. https://doi.org/10.1016/j.jsames.2024.104863

Altenhofen, S. D., Schrank, A. B. S., Dos Santos, T., Trombetta, M. C., Freitas, W. S., Cembrani, E., Simon, S. P., Martiny, J., Dalla

Vecchia, F., Maraschin, A. J., Barili, R., Rodrigues, A. G., & De Ros, L. F. (2026). Distribution of intraclastic deposits in the Barra Velha Formation, Santos Basin pre-salt: implications for the reworking processes. *Petroleum Geoscience*, *32*(1). https://doi.org/10.1144/petgeo2025-074

Apel, J. R., Ostrovsky, L. A., Stepanyants, Y. A., & Lynch, J. F. (2007). Internal solitons in the ocean and their effect on underwater sound. *The Journal of the Acoustical Society of America*, *121*(2), 695–722. https://doi.org/10.1121/1.2395914

Araújo, C. C., Madrucci, V., Homewood, P., Mettraux, M., Ramnani, C. W., & Spadini, A. R. (2022). Stratigraphic and sedimentary constraints on presalt carbonate reservoirs of the South Atlantic Margin, Santos Basin, offshore Brazil. *AAPG Bulletin*, *106*(12), 2513–2546. https://doi.org/10.1306/08082219218

Bádenas, B., Pomar, L., Aurell, M., & Morsilli, M. (2012). A facies model for internalites (internal wave deposits) on a gently sloping carbonate ramp (Upper Jurassic, Ricla, NE Spain). *Sedimentary Geology*, *271–272*, 44–57. https://doi.org/10.1016/j.sedgeo.2012.05.020

Barnett, A. J., Obermaier, M., Amthor, J., Sharafodin, M., Bolton, M., Clarke, D., & Camara, R. (2021). Chapter 6: Origin and Significance of Thick Carbonate Grainstone Packages in Nonmarine Successions: A Case Study from the Barra Velha Formation, Santos Basin, Brazil. *Memoir 124: The Supergiant Lower Cretaceous Pre-Salt Petroleum Systems of the Santos Basin, Brazil*, 155–174. https://doi.org/10.1306/13722318MSB.6.1853

Basso, M., Chinelatto, G. F., Belila, A. M. P., Mendes, L. C., Souza, J. P. P., Stefanelli, D., Vidal, A. C., & Bueno, J. F. (2023). Characterization of silicification and dissolution zones by integrating borehole image logs and core samples: a case study of a well from the Brazilian pre-salt. *Petroleum Geoscience*, *29*(3). https://doi.org/10.1144/petgeo2022-044

Budd, D. A. (2002). The Relative Roles of Compaction and Early Cementation in the Destruction of Permeability in Carbonate Grainstones: A Case Study from the Paleogene of West-Central Florida, U.S.A. *Journal of Sedimentary Research*, *72*(1), 116–128. https://doi.org/10.1306/061501720116

Carramal, N. G., Oliveira, D. M., Cacela, A. S. M., Cuglieri, M. A. A., Rocha, N. P., Viana, S. M., Toledo, S. L. V., Pedrinha, S., & de Ros, L. F. (2022). Paleoenvironmental insights from the deposition and diagenesis of Aptian pre-salt magnesium silicates from the Lula Field, Santos Basin, Brazil. *Journal of Sedimentary Research*, *92*(1), 12–31. https://doi.org/10.2110/jsr.2020.139

Carvalho, A. M. A., Hamon, Y., Gomes De Souza, O., Goulart Carramal, N., & Collard, N. (2022). Facies and diagenesis distribution in an Aptian pre-salt carbonate reservoir of the Santos Basin, offshore Brazil: A comprehensive quantitative approach. *Marine and Petroleum Geology*, *141*, 105708. https://doi.org/10.1016/j.marpetgeo.2022.105708

Choquette, P. W., & Pray, L. C. (1970). Geologic Nomenclature and Classification of Porosity in Sedimentary Carbonates. *AAPG Bulletin*, *54*(2), 207–250. https://doi.org/10.1306/5d25c98b-16c1-11d7-8645000102c1865d

Christ, A.-B., Cacas-Stentz, M.-C., Collard, N., Nader, F. H., Bemer, E., Bunevich, R. B., Borges Gomes, J. P., Gomes de Souza, O., & Abreu de Almeida dos Reis, M. A. (2025). Integrated 3D forward stratigraphic and basin modeling of the Santos Basin, offshore Brazil: Implications of sedimentary depositional facies and CO2 migration for silicification of continental carbonate reservoirs. *Marine and Petroleum Geology*, *180*, 107455. https://doi.org/10.1016/j.marpetgeo.2025.107455

De Medeiros, R. S. P., Basso, M., Chinelatto, G. F., Theodoro Soares, M. V., Matheus, G. F., Villacreses Morales, J. F., de Carvalho Mendes, L., & Vidal, A. C. (2024). Unravelling the origin of reworked deposits in Aptian lacustrine carbonate reservoirs of the Santos Basin, SE Brazil. *Marine and Petroleum Geology*, *161*, 106700. https://doi.org/10.1016/j.marpetgeo.2024.106700

De Oliveira Nardi Leite, C., De Assis Silva, C. M., & De Ros, L. F. (2020). Depositional and diagenetic processes in the pre-salt rift section of a Santos Basin area, SE Brazil. *Journal of Sedimentary Research*, *90*(6), 584–608. https://doi.org/10.2110/jsr.2020.27

De Ros, L. F. (2018). *Genesis and Evolution of Aptian Pre-salt Carbonate Reservoirs in Southeastern Brazilian Margin*. Brazilian Petroluem Conference, Rio de Janerio, Brazil. https://doi.org/10.13140/RG.2.2.12290.09922

De Ros, L. F. (2021). Syngenetic, Diagenetic and Hydrothermal Processes in the Pre-Salt Sag Section of Santos and Campos Basins. *Second EAGE Conference on Pre-Salt Reservoir*, *2021*, 1–5. https://doi.org/10.3997/2214-4609.202183007

De Ros, L. F., & Goldberg, K. (2007). *Reservoir petrofacies: A tool for quality characterization and prediction*. AAPG Annual Convention and Exhibition, Long Beach, California, USA.

De Ros, L. F., Goldberg, K., Abel, M., Victorinetti, F., Mastella, L., & Castro, E. (2007). *Advanced Acquisition and Management of Petrographic Information from Reservoir Rocks Using the PETROLEDGE® System*. AAPG Annual Convention and Exhibition, Long Beach, California, USA.

De Ros, L. F., & Oliveira, D. M. (2023). An operational classification system for the South Atlantic pre-salt rocks. *Journal of Sedimentary Research*, *93*(10), 693–704. https://doi.org/10.2110/jsr.2022.103

Deocampo, D. M. (2015). Authigenic clay minerals in lacustrine mudstones. In D. Larsen, S. O. Egenhoff, & N. S. Fishman (Eds.), *Paying Attention to Mudrocks: Priceless! Special Papers: 515* (pp. 49–64). Geological Society of America. https://doi.org/10.1130/2015.2515(03)

Dias, J. L. (2005). Tectônica, estratigrafia e sedimentação no andar Aptiano da margem leste brasileira. *Boletim de Geociências Da Petrobras*, *13*(1), 7–25. https://bgp.petrobras.com.br/bgp/article/view/207/

Dickson, J. A. D. (1965). A Modified Staining Technique for Carbonates in Thin Section. *Nature*, *205*, 587–587. https://doi.org/10.1038/205587a0

Ehrenberg, S. N. (1995). Measuring sandstone compaction from modal analyses of thin sections; how to do it and what the results mean. *Journal of Sedimentary Research*, *65*(2a), 369–379. https://doi.org/10.1306/D42680C7-2B26-11D7-8648000102C1865D

Farias, F., Szatmari, P., Bahniuk, A., & França, A. B. (2019). Evaporitic carbonates in the pre-salt of Santos Basin – Genesis and tectonic implications. *Marine and Petroleum Geology*, *105*, 251–272. https://doi.org/10.1016/j.marpetgeo.2019.04.020

Fernández-Ibáñez, F., Jones, G. D., Mimoun, J. G., Bowen, M. G., Simo, J. A. ., Marcon, V., & Esch, W. L. (2022). Excess permeability in the Brazil pre-Salt: Nonmatrix types, concepts, diagnostic indicators, and reservoir implications. *AAPG Bulletin*, *106*(4), 701–738. https://doi.org/10.1306/10042120171

Fernández-Ibáñez, F., Nolting, A., Breithaupt, C. I., Darby, B., Mimoun, J., & Henares, S. (2022). The properties of faults in the Brazil pre-salt: A reservoir characterization perspective. *Marine and Petroleum Geology*, *146*, 105955. https://doi.org/10.1016/j.marpetgeo.2022.105955

Fragoso, D. G. C., De Melo, A. H., Gonçalves, L. A., Bunevich, R. B., De Aratanha Maia Araujo, J., Da Costa, T. C., Pedrosa, C. A., & Dos Santos Scherer, C. M. (2023). High-resolution sequence stratigraphy applied to reservoir characterization of the Brazilian Cretaceous pre-salt section, Campos Basin: Guidelines for geological modeling and reservoir management. *Marine and Petroleum Geology*, *151*, 106203. https://doi.org/10.1016/j.marpetgeo.2023.106203

Goldstein, R. H. (2001). Fluid inclusions in sedimentary and diagenetic systems. *Lithos*, *55*(1–4), 159–193. https://doi.org/10.1016/S0024-4937(00)00044-X

Goldstein, R. H., & Reynolds, T. J. (Eds.). (1994). *Systematics of Fluid Inclusions in Diagenetic Minerals: Short Course Notes: 31*. SEPM Society for Sedimentary Geology. https://doi.org/10.2110/scn.94.31

Gomes, J. P. B., Bunevich, R. B., Sartorato, A. C. L., Tedeschi, L. R., Tonietto, S. N., Tucker, M. E., & Whitaker, F. (2024). Early diagenetic evolution based on petrography and stable isotope analysis in the Barra Velha Formation of the Brazilian Pre-salt. *The Depositional Record*, *11*(1), 70–94. https://doi.org/10.1002/dep2.288

Gomes, J. P. B., Bunevich, R. B., Tedeschi, L. R., Tucker, M. E., & Whitaker, F. F. (2020). Facies classification and patterns of lacustrine carbonate deposition of the Barra Velha Formation, Santos Basin, Brazilian Pre-salt. *Marine and Petroleum Geology*, *113*, 104176. https://doi.org/10.1016/j.marpetgeo.2019.104176

Guo, P., Wen, H., Li, C., He, H., & Sánchez-Román, M. (2023). Lacustrine dolomite in deep time: What really matters in early dolomite formation and accumulation? *Earth-Science Reviews*, *246*, 104575. https://doi.org/10.1016/j.earscirev.2023.104575

Guzzo, J., Rocha, Y., Menezes, T., Pestilho, A. L., Binotto, R., Matos, T., Silva, Y., Tonietto, S., Filho, R., & Carvalho, B. (2018, November 4). *Hydrothermal petroleums and solid reservoir bitumens: recognition of an atypical petroleum system in the Brazilian Pre-salt deposits (Santos Basin)*. XV Latin American Congress on Organic Geochemistry.

Herlinger, R., De Ros, L. F., Surmas, R., & Vidal, A. (2023). Residual oil saturation investigation in Barra Velha Formation reservoirs from the Santos Basin, Offshore Brazil: A sedimentological approach. *Sedimentary Geology*, *448*, 106372. https://doi.org/10.1016/j.sedgeo.2023.106372

Herlinger, R., Zambonato, E. E., & De Ros, L. F. (2017). Influence of Diagenesis On the Quality of Lower Cretaceous Pre-salt Lacustrine Carbonate Reservoirs from Northern Campos Basin, Offshore Brazil. *Journal of Sedimentary Research*, *87*(12), 1285–1313. https://doi.org/10.2110/jsr.2017.70

Hirst, J. F. (1995). *Sedimentology, diagenesis and hydrochemistry of the saline, alkaline lakes on the Cariboo Plateau, interior British Columbia, Canada* [Master thesis, University of Saskatchewan]. http://hdl.handle.net/10388/etd-10252012-134220

Immenhauser, A. (2021). On the delimitation of the carbonate burial realm. *The Depositional Record*, *8*(2), 524–574. https://doi.org/10.1002/dep2.173

Lapponi, F., Hunt, D. W., & Dickinson, T. (2019). *Low and high temperature silica diagenesis in a giant pre-salt reservoir: BM-C-33, Campos Basin, Brazil*. First EAGE Workshop on Pre-Salt Reservoir: From Exploration to Production. https://doi.org/10.3997/2214-4609.201982017

Last, W. M. (1990). Lacustrine dolomite—an overview of modern, Holocene, and Pleistocene occurrences. *Earth-Science Reviews*, *27*(3), 221–263. https://doi.org/10.1016/0012-8252(90)90004-F

Li, C., Guo, P., Zhong, K., Xu, J., & Wen, H. (2023). Formation and diagenesis of authigenic silicates in the Late Paleozoic alkaline lake deposits, Junggar Basin, NW China. *Sedimentary Geology*, *458*, 106531. https://doi.org/10.1016/j.sedgeo.2023.106531

Lima, B. E. M., & De Ros, L. F. (2019). Deposition, diagenetic and hydrothermal processes in the Aptian Pre-Salt lacustrine carbonate reservoirs of the northern Campos Basin, offshore Brazil. *Sedimentary Geology*, *383*, 55–81. https://doi.org/10.1016/j.sedgeo.2019.01.006

Lima, B. E. M., Tedeschi, L. R., Pestilho, A. L. S., Santos, R. V., Vazquez, J. C., Guzzo, J. V. P., & De Ros, L. F. (2020). Deep-burial hydrothermal alteration of the Pre-Salt carbonate reservoirs from northern Campos Basin, offshore Brazil: Evidence from petrography, fluid inclusions, Sr, C and O isotopes. *Marine and Petroleum Geology*, *113*, 104143. https://doi.org/10.1016/j.marpetgeo.2019.104143

Machel, H.-G. (1987). Saddle dolomite as a by-product of chemical compaction and thermochemical sulfate reduction. *Geology*, *15*(10), 936. https://doi.org/10.1130/0091-7613(1987)15<936:SDAABO>2.0.CO;2

Magoon, L. B., & Dow, W. G. (1994). The Petroleum System. In L. B. Magoon & W. G. Dow (Eds.), *The Petroleum System—From Source to Trap: Memoir: 60* (pp. 3–24). American Association of Petroleum Geologists. https://doi.org/10.1306/M60585C1

Mohriak, W., Nemčok, M., & Enciso, G. (2008). South Atlantic divergent margin evolution: rift-border uplift and salt tectonics in the basins of SE Brazil. In R. A. J. Trouw, B. B. de Brito Neves, & M. J. de Wit (Eds.), *West Gondwana: Pre-Cenozoic Correlations Across the South Atlantic Region: Special Publications: 294* (pp. 365–398). Geological Society of London. https://doi.org/10.1144/SP294.19

Morad, S., Al-Aasm, I. S., Nader, F. H., Ceriani, A., Gasparrini, M., & Mansurbeg, H. (2012). Impact of diagenesis on the spatial and temporal distribution of reservoir quality in the Jurassic Arab D and C members, offshore Abu Dhabi oilfield, United Arab Emirates. *GeoArabia*, *17*(3), 17–56. https://doi.org/10.2113/geoarabia170317

Moreira, J. L. P., Madeira, C. V., Gil, J. A., & Machado, M. A. P. (2007). Bacia de Santos. *Boletim de Geociências Da Petrobras*, *15*(2), 531–549. https://bgp.petrobras.com.br/bgp/article/view/354

Pietzsch, R., Oliveira, D. M., Tedeschi, L. R., Queiroz Neto, J. V., Figueiredo, M. F., Vazquez, J. C., & de Souza, R. S. (2018). Palaeohydrology of the Lower Cretaceous pre-salt lacustrine system, from rift to post-rift phase, Santos Basin, Brazil. *Palaeogeography, Palaeoclimatology, Palaeoecology*, *507*, 60–80. https://doi.org/10.1016/j.palaeo.2018.06.043

Pietzsch, R., Tedeschi, L. R., Oliveira, D. M., dos Anjos, C. W. D., Vazquez, J. C., & Figueiredo, M. F. (2020). Environmental conditions of deposition of the Lower Cretaceous lacustrine carbonates of the Barra Velha Formation, Santos Basin (Brazil), based on stable carbon and oxygen isotopes: A continental record of pCO2 during the onset of the Oceanic Anoxic Event 1a (OAE 1a) interval? *Chemical Geology*, *535*, 119457. https://doi.org/10.1016/j.chemgeo.2019.119457

Platt, N. H., & Wright, V. P. (1991). Lacustrine Carbonates: Facies Models, Facies Distributions and Hydrocarbon Aspects. In P. Anadón, L. Cabrera, & K. Kelts (Eds.), *Lacustrine Facies Analysis: Special Publication of the International Association of Sedimentologists: 13*. International Association of Sedimentologists/Wiley. https://doi.org/10.1002/9781444303919.ch3

Pomar, L., Morsilli, M., Hallock, P., & Bádenas, B. (2012). Internal waves, an under-explored source of turbulence events in the sedimentary record. *Earth-Science Reviews*, *111*(1–2), 56–81. https://doi.org/10.1016/j.earscirev.2011.12.005

Poros, Z., Jagniecki, E., Luczaj, J., Kenter, J., Benedek, G., Correa, T. S., Ferreira, E., McFadden, K. A., Elifritz, A., Heumnann, M., Johnston, M., & Matt, V. (2017). *Origin of silica in pre-salt carbonates, Kwanza Basin, Angola*. AAPG 2017 Annual Convention and Exhibition. https://www.searchanddiscovery.com/documents/2017/51413poros/ndx_poros.pdf

Preusse, M., Peeters, F., & Lorke, A. (2010). Internal waves and the generation of turbulence in the thermocline of a large lake. *Limnology and Oceanography*, *55*(6), 2353–2365. https://doi.org/10.4319/lo.2010.55.6.2353

Quirk, D. G., Hertle, M., Jeppesen, J. W., Raven, M., Mohriak, W. U., Kann, D. J., Nørgaard, M., Howe, M. J., Hsu, D., Coffey, B., & Mendes, M. P. (2013). Rifting, subsidence and continental break-up above a mantle plume in the central South Atlantic. In W. U. Mohriak, A. Danforth, P. J. Post, D. E. Brown, G. C. Tari, M. Nemčok, & S. T. Sinha (Eds.), *Conjugate Divergent Margins: Special Publications: 369* (pp. 185–214). Geological Society of London. https://doi.org/10.1144/SP369.20

Roedder, E. (1984). *Fluid inclusions: Reviews in Mineralogy: 12*. Mineralogical Society of America. https://doi.org/10.1515/9781501508271

Rossoni, R. B., Porcher, C. C., Koester, E., Sobiesiak, J. S., Da Silva, L. A. C., Mexias, A. S., Gomes, M. E. B., Ramnani, C. W., & De Ros, L. F. (2024). The role of compaction in the diagenetic evolution of Pre-Salt Aptian deposits of Santos Basin, Brazil. *Sedimentary Geology*, *466*, 106650. https://doi.org/10.1016/j.sedgeo.2024.106650

Sabato Ceraldi, T., & Green, D. (2016). Evolution of the South Atlantic lacustrine deposits in response to Early Cretaceous rifting, subsidence and lake hydrology. In T. S. Ceraldi, R. A. Hodgkinson, & G. Backe (Eds.), *Petroleum Geoscience of the West Africa Margin: Special Publications: 438* (pp. 77–98). Geological Society of London. https://doi.org/10.1144/SP438.10

Saller, A., Rushton, S., Buambua, L., Inman, K., McNeil, R., & Dickson, J. A. D. . (2016). Presalt stratigraphy and depositional systems in the Kwanza Basin, offshore Angola. *AAPG Bulletin*, *100*(07), 1135–1164. https://doi.org/10.1306/02111615216

Sartorato, A. C. L., Tonietto, S. N., & Pereira, E. (2020). Silicification and dissolution features in the brazilian Pre-salt Barra Velha formation: impacts in the reservoir quality and insights for 3D geological modeling. *Rio Oil and Gas Expo and Conference*, *20*(2020), 68–69. https://doi.org/10.48072/2525-7579.rog.2020.068

Schmidt, J., Cembrani, E., Dos Santos, T., Trombetta, M. C., Lenz, R., Schrank, A., Altenhofen, S., Rodrigues, A., De Ros, L., Dalla Vecchia, F., & Barili, R. (2025). Petrography and Fluid Inclusions for Petroleum System Analysis of Pre-Salt Reservoirs in the Santos Basin, Eastern Brazilian Margin. *Geosciences*, *15*(5), 158. https://doi.org/10.3390/geosciences15050158

Schrank, A. B. S., Dos Santos, T., Altenhofen, S. D., Freitas, W., Cembrani, E., Haubert, T., Dalla Vecchia, F., Barili, R., Rodrigues, A. G., Maraschin, A., & De Ros, L. F. (2024). Interactions between Clays and Carbonates in the Aptian Pre-Salt Reservoirs of Santos Basin, Eastern Brazilian Margin. *Minerals*, *14*(2), 191. https://doi.org/10.3390/min14020191

Spötl, C., & Pitman, J. K. (1998). Saddle (Baroque) Dolomite in Carbonates and Sandstones: A Reappraisal of a Burial-Diagenetic Concept. In S. Morad (Ed.), *Carbonate Cementation in Sandstones: Distribution Patterns and Geochemical Evolution* (pp. 437–460). International Association of Sedimentologists/Wiley. https://doi.org/10.1002/9781444304893.ch19

Szatmari, P., & Milani, E. J. (2016). Tectonic control of the oil-rich large igneous-carbonate-salt province of the South Atlantic rift. *Marine and Petroleum Geology*, *77*, 567–596. https://doi.org/10.1016/j.marpetgeo.2016.06.004

Teboul, P.-A., Durlet, C., Girard, J.-P., Dubois, L., San Miguel, G., Virgone, A., Gaucher, E. C., & Camoin, G. (2019). Diversity and origin of quartz cements in continental carbonates: Example from the Lower Cretaceous rift deposits of the South Atlantic margin. *Applied Geochemistry*, *100*, 22–41. https://doi.org/10.1016/j.apgeochem.2018.10.019

Terra, G. J. S., Spadini, A. R., França, A. B., Sombra, C. L., Zambonato, E. E., Juschaks, L. C. da S., Arienti, L. M., Franco, M. P., Erthal, M. M., Blauth, M., Matsuda, N. S., Silva, N. G. C. da, Moretti Jnr, P. A., D'Avila, R. S. F., Souza, R. S. de, Tonietto, S. N., Anjos, S. M. C. dos, Campinho, V. S., & Winter, W. R. (2010). Classificação de rochas carbonáticas aplicável às bacias sedimentares brasileiras. *Boletim de Geociências Da Petrobras*, *18*(1), 9–29. https://bgp.petrobras.com.br/bgp/article/view/113

Tosca, N. J., & Masterson, A. L. (2014). Chemical controls on incipient Mg-silicate crystallization at 25°C: Implications for early and late diagenesis. *Clay Minerals*, *49*(2), 165–194. https://doi.org/10.1180/claymin.2014.049.2.03

Tosca, N. J., & Tutolo, B. M. (2023). Hydrothermal vent fluid-seawater mixing and the origins of Archean iron formation. *Geochimica et Cosmochimica Acta*, *352*, 51–68. https://doi.org/10.1016/j.gca.2023.05.002

Tosca, N. J., & Wright, V. P. (2015). Diagenetic pathways linked to labile Mg-clays in lacustrine carbonate reservoirs: a model for the origin of secondary porosity in the Cretaceous pre-salt Barra Velha Formation, offshore Brazil. In P. J. Armitage, A. R. Butcher, J. M. Churchill, A. E. Csoma, C. Hollis, R. H. Lander, J. E. Omma, & R. H. Worden (Eds.), *Reservoir Quality of Clastic and Carbonate Rocks: Analysis, Modelling and Prediction: Special Publications: 435* (pp. 33–46). Geological Society of London. https://doi.org/10.1144/SP435.1

Tucker, M. E., & Wright, V. Paul. (2009). *Carbonate sedimentology*. Wiley-Blackwell. https://doi.org/10.1002/9781444314175

Tutolo, B. M., & Tosca, N. J. (2018). Experimental examination of the Mg-silicate-carbonate system at ambient temperature: Implications for alkaline chemical sedimentation and lacustrine carbonate formation. *Geochimica et Cosmochimica Acta*, *225*, 80–101. https://doi.org/10.1016/j.gca.2018.01.019

Wennberg, O. P., McQueen, G., Vieira de Luca, P. H., Lapponi, F., Hunt, D., Chandler, A. S., Waldum, A., Nery Camargo, G., Castro, E., & Loures, L. (2021). Open fractures in pre-salt silicified carbonate reservoirs in block BM-C-33, the Outer Campos Basin, offshore Brazil. *Petroleum Geoscience*, *27*(4). https://doi.org/10.1144/petgeo2020-125

Wright, V. P. (2012). Lacustrine carbonates in rift settings: the interaction of volcanic and microbial processes on carbonate deposition. In J. Garland, J. E. Neilson, S. E. Laubach, & K. J. Whidden (Eds.), *Advances in Carbonate Exploration and Reservoir Analysis: Special Publications: 370*. Geological Society of London. https://doi.org/10.1144/SP370.2

Wright, V. P. (2022). The mantle, CO_2 and the giant Aptian chemogenic lacustrine carbonate factory of the South Atlantic: Some carbonates are made, not born. *Sedimentology*, *69*(1), 47–73. https://doi.org/10.1111/sed.12835

Wright, V. P., & Barnett, A. J. (2015). An abiotic model for the development of textures in some South Atlantic early Cretaceous lacustrine carbonates. In D. W. J. Bosence, K. A. Gibbons, D. P. Le Heron, W. A. Morgan, T. Pritchard, & B. A. Vining (Eds.), *Microbial Carbonates in Space and Time: Implications for Global Exploration and Production: Special Publications: 418* (pp. 209–219). Geological Society of London. https://doi.org/10.1144/SP418.3

Wright, V. P., & Barnett, A. J. (2017). *Critically Evaluating the Current Depositional Models for the Pre-Salt Barra Velha Formation, Offshore Brazil*. AAPG Datapages: Search and Discovery (90310). AAPG/SEG International Conference and Exhibition, London, England. https://www.searchanddiscovery.com/abstracts/pdf/2017/90310aapg/abstracts/ndx_wright.pdf

Wright, V. P., & Rodriguez, K. (2018). Reinterpreting the South Atlantic Pre-Salt 'Microbialite' reservoirs: petrographic, isotopic and seismic evidence for a shallow evaporitic lake depositional model. *First Break*, *36*(5), 71–77. https://doi.org/10.3997/1365-2397.n0094

Wright, V. P., & Tosca, N. J. (2016). *A geochemical model for the formation of the pre-salt reservoirs, Santos Basin, Brazil: Implications for understanding reservoir distribution*. AAPG Datapages: Search and Discovery (51304). AAPG Annual Convention & Exhibition, Calgary, Alberta, Canada. https://www.searchanddiscovery.com/documents/2016/51304wright/ndx_wright.pdf